



Mapping the human middle longitudinal fasciculus through a focused anatomo-imaging study: shifting the paradigm of its segmentation and connectivity pattern

Aristotelis Kalyvas^{1,2,5} · Christos Koutsarnakis^{1,2,5} · Spyridon Komaitis^{1,2,5} · Efstratios Karavasilis³ · Foteini Christidi⁴ · Georgios P. Skandalakis^{1,5} · Evangelia Liouta^{1,6} · Olympia Papakonstantinou³ · Nikolaos Kelekis³ · Hugues Duffau⁷ · George Stranjalis^{1,2,6}

Received: 29 May 2019 / Accepted: 14 November 2019 / Published online: 26 November 2019
© Springer-Verlag GmbH Germany, part of Springer Nature 2019

Abstract

The middle longitudinal fasciculus (MdLF) was initially identified in humans as a discrete subcortical pathway connecting the superior temporal gyrus (STG) to the angular gyrus (AG). Further anatomo-imaging studies, however, proposed more sophisticated but conflicting connectivity patterns and have created a vague perception on its functional anatomy. Our aim was, therefore, to investigate the ambiguous structural architecture of this tract through focused cadaveric dissections augmented by a tailored DTI protocol in healthy participants from the Human Connectome dataset. Three segments and connectivity patterns were consistently recorded: the MdLF-I, connecting the dorsolateral Temporal Pole (TP) and STG to the Superior Parietal Lobule/Precuneus, through the Heschl's gyrus; the MdLF-II, connecting the dorsolateral TP and the STG with the Parieto-occipital area through the posterior transverse gyri and the MdLF-III connecting the most anterior part of the TP to the posterior border of the occipital lobe through the AG. The lack of an established termination pattern to the AG and the fact that no significant leftward asymmetry is disclosed tend to shift the paradigm away from language function. Conversely, the theory of “where” and “what” auditory pathways, the essential relationship of the MdLF with the auditory cortex and the functional role of the cortical areas implicated in its connectivity tend to shift the paradigm towards auditory function. Allegedly, the MdLF-I and MdLF-II segments could underpin the perception of auditory representations; whereas, the MdLF-III could potentially subserve the integration of auditory and visual information.

Keywords Middle longitudinal fasciculus · Brain connectivity · Occipital lobe · Temporal pole · Temporal lobe · Auditory function

Aristotelis Kalyvas and Christos Koutsarnakis contributed equally in this study.

Electronic supplementary material The online version of this article (<https://doi.org/10.1007/s00429-019-01987-6>) contains supplementary material, which is available to authorized users.

✉ Christos Koutsarnakis
ckouts@hotmail.co.uk

¹ Athens Microneurosurgery Laboratory, Evangelismos Hospital, Athens, Greece

² Department of Neurosurgery, Evangelismos Hospital, National and Kapodistrian University of Athens, Athens, Greece

³ Second Department of Radiology, Attikon Hospital, National and Kapodistrian University of Athens, Athens, Greece

Introduction

Anatomical investigations by early scientists have sparked interest in cerebral subcortical anatomy and paved the way for a fundamental change in our perception of the white

⁴ First Department of Neurology, Aeginition Hospital, National and Kapodistrian University of Athens, Athens, Greece

⁵ Department of Anatomy, Medical School, National and Kapodistrian University of Athens, Athens, Greece

⁶ Hellenic Center for Neurosurgical Research, “PetrosKokkalis”, Athens, Greece

⁷ Department of Neurosurgery, Montpellier University Medical Center, Gui de Chauliac Hospital, Montpellier, France

matter, from being regarded as an amorphous mass, to actually represent a complex network of tracts that interconnect adjacent and distant cortical and subcortical areas (Schmahmann and Pandya 2007). Later, the introduction of Klingler's technique refined the anatomical investigation of white matter microstructure through the fixation of brains in a formalin solution followed by a freeze–thaw process, which facilitates meticulous dissections and enhances the delineation of fiber pathways (Klingler 1935; Klingler and Ludwig 1956). Further, the recent advent of diffusion-weighted magnetic resonance imaging has allowed for a fast and non-invasive investigation of the white matter architecture *in vivo*, and has provided valuable insights on the intrinsic white matter anatomy and its 3D representation (Basser et al. 1994; Catani and De Schotten 2008; Catani et al. 2002; Le Bihan et al. 2001; Mori and Zhang 2006; Schmahmann et al. 2007).

From a functional standpoint, evidence from stroke studies combined with data stemming from pathologic processes mainly affecting white matter structures, such as multiple sclerosis, have led to the appreciation of a broad clinical significance of the cerebral white matter (Filley 1998, 2005). Keeping with this, functional neuroimaging (Logothetis et al. 2001; Maldjian et al. 2003; Price 2000; Yang et al. 2016) and human brain mapping studies (Duffau 2011; Duffau and Duffau 2010; Mazziotta et al. 2001; Raichle 2009; Sarubbo et al. 2015; Sporns et al. 2005) reflect the concept of a cortico-subcortical correlation and integration, thus emphasizing on a hodotopical network approach to understand higher cerebral processing (Catani and Catani 2007; De Benedictis and Duffau 2011). To this end, advances in decoding the anatomical basis of cerebral processing along with the availability of the non-invasive diffusion tensor imaging (DTI) technique led to a special research interest on the white matter architecture and brain connectivity. Due to specific technical limitations of DTI and tractography, data had to be validated through classical anatomic descriptions of white matter tracts (Dejerine and Dejerine-Klumpke 1895; Makris et al. 1999) or alternatively be compared to relevant studies on non-human primates (Makris et al. 2009). However, especially with regard to novel tracts, neither of the two aforementioned approaches seems to be accurate (Koutsarnakis et al. 2019; Rilling et al. 2008). Hence, the Klingler's technique is currently considered as the gold standard method through which DTI results can be verified (Mandonnet et al. 2018).

We, therefore, opted to study through a combined approach entailing white matter anatomic dissections and DTI tractography the architecture of a fiber tract known as the Middle Longitudinal Fasciculus (MdLF). Although this bundle was originally described in macaque monkeys by Seltzer and Pandya (1984), it was not until 2009 that Makris et al. provided preliminary supporting DTI evidence of its existence and connectivity in the human brain (Makris et al.

2009). Further DTI studies that aimed to enhance our knowledge on MdLF subcortical architecture introduced ambiguity instead by suggesting more sophisticated but at the same time conflicting connectivity patterns (Conner et al. 2018; Makris et al. 2013a, b; 2017; Menjot de Champfleury et al. 2013; Tremblay et al. 2019). In the same vein, discrepancy remains even in the two available studies that employed microanatomic techniques to explore the morphology and inherent configuration of the MdLF (Maldonado et al. 2013; Wang et al. 2013).

Our objective was, therefore, to clarify the debatable anatomical characteristics of the MdLF through focused dissections augmented by a tailored DTI protocol. Dissections were the core analysis approach of our study and DTI was used as a complementary method which was applied on an independent sample of healthy adults from the publicly available dataset of the Human Connectome Project (<http://humanconnectome.org>). In addition, we provide a review of the pertinent anatomo-tractographic literature with the overarching goal to compare our findings with current data and further provide insights on the MdLF structure to function relationship.

Methods

White matter dissection

Twenty adult, normal, cadaveric cerebral hemispheres (9 right hemispheres–11 left hemispheres) obtained from 20 different cadavers previously fixed by immersion in a 10–15% formalin solution for a minimum period of 8 weeks were included. Following careful removal of the arachnoid membrane and vessels, the specimens were initially refrigerated at temperatures between – 10 and – 15 for 15 days and were then allowed to thaw under running water for several hours (Klingler or freeze–thaw procedure). Subsequently, all cerebral hemispheres were investigated using the fiber dissection technique and the operating microscope (Carl Zeiss OPMIR Plus, Carl Zeiss AG, Oberkochen, Germany) (Klingler 1935; Klingler and Ludwig 1956; Koutsarnakis et al. 2015; Martino et al. 2011; Ture et al. 2000).

According to current literature, the MdLF runs in the lateral aspect of the hemisphere and participates in the axonal connectivity of the superior temporal gyrus (STG) and the parietal and occipital lobes (Conner et al. 2018; Makris et al. 2009, 2013a, b, 2017; Maldonado et al. 2013; Menjot de Champfleury et al. 2013; Wang et al. 2013). We, therefore, performed lateral to medial anatomic dissections with special emphasis on the aforementioned area. To better illustrate the subcortical correlative anatomy, we further dissected the entire temporal lobe, insula and fronto-parietal operculum.

Prior to the dissection process, the sulcal and gyral anatomy of the lateral aspect of the hemisphere was recorded in detail.

DTI imaging

For the purpose of the present study, we used data from the Human Connectome Project database (<https://ida.loni.usc.edu/login.jsp>). The Human Connectome Project (Principal Investigators: Bruce Rosen, M.D., Ph.D., Martinos Center at Massachusetts General Hospital; Arthur W. Toga, Ph.D., University of Southern California, Van J. Weeden, MD, Martinos Center at Massachusetts General Hospital) is supported by the National Institute of Dental and Craniofacial Research, the National Institute of Mental Health and the National Institute of Neurological Disorders and Stroke. HCP is the result of efforts of co-investigators from the University of Southern California, Martinos Center for Biomedical Imaging at Massachusetts General Hospital, Washington University, and the University of Minnesota.

Thirty-five (35) healthy participants (mean age = 31.1 years, (20–59 years old); 16 females/19 males) from the MGH-USC Adult Diffusion Dataset (Human Connectome available dataset) underwent brain imaging in a 3-Tesla CONNECTOM magnetic resonance imaging (MRI) scanner (Setsompop et al. 2013) housed at the MGH/HST Athinoula A. Martinos Center for Biomedical Imaging with a custom-made 64-channel phased array head coil (Keil et al. 2013). Anatomic imaging was performed with a 1-mm isotropic Multi-echo Magnetization-Prepared Rapid Acquisition Gradient Echo three-dimensional T1-weighted sequence. DTI parameters included an axial spin-echo multi-band echo-planar imaging sequence with 64 diffusion encoding directions; field of view: 210 mm; acquisition voxel size: $1.5 \times 1.5 \times 1.5$ mm³; repetition time: 8800 ms; echo time: 57 ms; b factors with 0 s/mm² (low b-value) and 1000 s/mm² (high b-value). The acquisition consisted of 96 slices.

DTI images were processed using the Brainance MD (Advantis Medical Imaging, Eindhoven, The Netherlands). A multiple region-of-interest (ROI) approach was applied on fractional anisotropy (FA) maps based on anatomical landmarks derived from previous white matter dissection and DTI studies to reconstruct the entire bundle of MdLF (Fig. 1). Specifically, the tracing of the ROIs was performed in coronal plane, using three different ROIs. The first two ROIs were placed at the level of the superior temporal gyrus. For the first ROI, the central sulcus was identified in the sagittal plane and then the area between the lateral fissure and the superior temporal sulcus including the Heschl's gyrus was selected on a coronal plane. The second ROI was placed six slices anterior to the first ROI using the same anatomical margins. For the third ROI, the mid-part of the parieto-occipital sulcus was identified in the sagittal plane and a ROI was placed in the coronal plane covering

the entire hemisphere, according to previous dissection and DTI studies (Conner et al. 2018; Makris et al. 2013a; 2017; Maldonado et al. 2013; Menjot de Champfleury et al. 2013; Wang et al. 2013) that support the parieto-occipital termination of MdLF fibers.

All tracts passing through these ROIs with a minimum FA of 0.15, maximum angle change of 27°, minimum length of 0 mm and maximum length of 200 mm were traced. The following DTI measures were then extracted for the entire MdLF and segments I–III of MdLF: mean fractional anisotropy (FA); mean axial diffusivity (AD); mean radial diffusivity (RD); number of fibers (NoF).

Concerning the topography of MdLF in relation to adjacent white matter tracts, we further reconstructed the following tracts: inferior longitudinal fasciculus (ILF), inferior fronto-occipital fasciculus (IFOF), superior longitudinal fasciculus (SLF) and uncinate fasciculus (UF). The reconstruction was based on a previous well-standardized protocol (Wakana et al. 2007) and software default threshold values for FA, angle change and fiber length.

All the reconstructed tracts were assessed by two experienced neuroradiologists. All DTI data were analyzed twice by a single experienced rater (EK) with an interval of 4 weeks, to assess intra-observer agreement. To determine inter-observer agreement for the MdLF and its segments, the same dataset was additionally analyzed by a second experienced rater (FC), who was blinded to the results of the first rater. Intra- and inter-rater agreement was evaluated within the group of healthy participants with intraclass correlation coefficient (ICC) (Shrout and Fleiss 1979). ICC values greater than 0.80 were found in all cases. Symmetry index (SI) was calculated for mean FA, AD and RD according to the formula: $(L - R)/(0.5 \times (L + R))$. The variability of FA, AD and RD of the reconstructed tracts for the left and right hemispheres is presented by coefficient of variability (CV) which is depicted as CV%, calculated as: $CV\% = (\text{standard deviation})/(\text{mean}) \times 100\%$. Pairwise comparisons were also conducted to test left–right differences at $p < 0.05$ (after Bonferroni correction for multiple comparisons), using IBM SPSS Statistics v. 20.

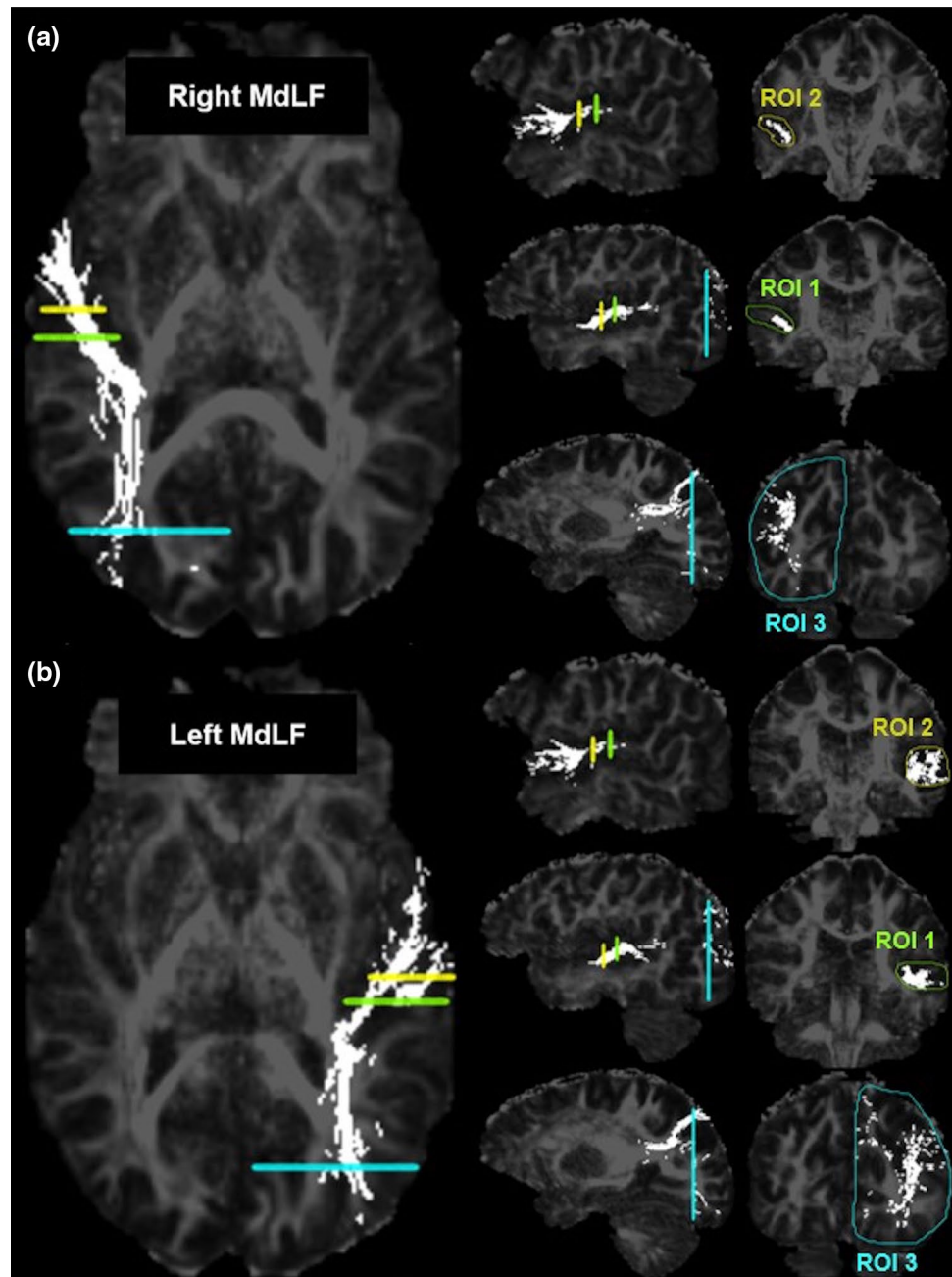
Results

White matter dissection

White matter dissection steps

Starting the dissection from the superior temporal sulcus (STS) and gyrus (STG), including the transverse gyri, we moved our plane posteriorly and superiorly towards the parieto-occipital area. Following the removal of cortical gray matter, the arcuate or U-fibers of the lateral aspect of the

Fig. 1 Representation of the multiple ROIs used for the reconstruction of the MdLF (entire bundle) in the right (a) and left (b) hemisphere and projection over an FA map in axial (left panel), sagittal (middle panel) and coronal (right panel) plane. The first two ROIs (colored in green and yellow, respectively) were placed at the level of the STG in coronal plane, whereas the third ROI (colored in cyan) was placed in coronal plane after the identification of the mid parieto-occipital sulcus in a sagittal plane and covered the entire hemisphere. *ROI* region of interest, *MdLF* middle longitudinal fasciculus, *FA* fractional anisotropy



hemisphere are evident (Step 1) (Fig. 2). These fibers connect adjacent gyri and form the most superficial layer of white matter. Removing the U-fibers of the inferior central lobe, inferior parietal lobule (IPL) and temporo-parieto-occipital (TPO) junction, discloses the superior longitudinal fasciculus (SLF)/arcuate fasciculus (AF) complex, which essentially connects the IFG and middle frontal gyrus (MFG) with the IPL and temporal lobe (Step 2) (Fig. 2). Dissecting the U-fibers of the STG and STS unveils a distinct group of fibers that originate from the temporal pole (TP) and anterior segment of the STS/STG and exhibit a horizontal trajectory, corresponding to the anterior part of

the MdLF (Step 3) (Fig. 3). The majority of the MdLF fibers were found to enter the transverse gyri and course upwards and posteriorly, just under the SLF/AF complex. Removing the SLF/AF complex helps to identify and record the parietal course of the MdLF. In this step, the insula and the most anterior part of the inferior frontal gyrus (IFG) were also included in the dissection with the aim to reveal the dorsal external capsule, the UF and IFOF and to differentiate them from the MdLF. More specifically, the U-fibers of the insula are dissected away to delineate the claustrorocortical fibers of the dorsal external capsule and to distinguish them from the MdLF. The U-fibers of the intraparietal sulcus (IPS) and

TPO junction were preserved to determine whether MdLF fibers change trajectory and terminate at the AG and SMG or instead head towards the SPL and occipital lobe. Not unexpectedly, MdLF fibers can be readily identified and differentiated from the dorsal external capsule fibers. Although these tracts exhibit the same direction (antero-inferior to postero-superior), the MdLF lies postero-laterally with respect to the dorsal external capsule, while their anterior origin is completely different, i.e., claustrum for the dorsal external capsule and STG for the MdLF. None of the MdLF fibers was seen to change trajectory and terminate to the angular gyrus (AG) and supramarginal gyrus (SMG). On the contrary, we found this part of the MdLF to pass deep to the IPL and to continue towards the SPL and occipital lobe. Interestingly, fibers stemming from the SLF were seen travelling through the IPS and finally terminating at the AG. Dissecting away the U-fibers of the IPS reveals fibers of the MdLF reaching the postero-superior part of the SPL and the parieto-occipital arcus (POA) (Alves et al. 2012; Maldonado et al. 2013; Rhoton Jr 2002). Removing the U-fibers of the TPO junction unveils MdLF fibers continuing further posteriorly to enter the occipital lobe (Step 4) (Fig. 4). In this dissection step, we recorded a discrete group of fibers, which were seen to run under the U-fibers of the occipital lobe and exhibit a vertical trajectory, corresponding to the Vertical Occipital Fasciculus (VOF). After removing the VOF, the stem of the MdLF was observed to course vertically and medially, in relation to the VOF, and was seen to reach the posterior border of the occipital lobe (Step 5) (Fig. 4). With regard to the anterior part of the MdLF, special attention was placed to the proper and careful dissection of the U-fibers of the anterior IFG and the anteriormost part of the temporal pole. Our aim was to disclose the UF, IFOF and ILF and to determine whether the most anterior part of the MdLF reaches the TP. Interestingly, the MdLF was consistently found to reach the anterior segment of the STG and the dorsal TP, while it was clearly demarcated and distinguished from the UF, IFOF and ILF. Following the complete exposure of the MdLF in the lateral cerebral aspect, we meticulously dissected, detached and retracted its fibers, starting from the TP and anterior STG, with the goal to record its connectivity and possibly identify a segmentation pattern (Step 6) (Fig. 5). Interestingly enough, the fibers originating at the dorsolateral TP were seen to travel through the transverse gyri to reach the SPL and the POA. More specifically, MdLF fibers entering the Heschl's gyrus, i.e., the first of the transverse temporal gyri in an anteroposterior direction, were documented to follow a superior trajectory and to terminate at the supero-posterior part of the SPL; while fibers travelling through the posterior transverse area were found to course obliquely to reach the more medially and posteriorly placed POA. In addition, fibers originating at the most anterior part of the TP and STS were identified to travel ventrally in the depth

of the STS, following a horizontal trajectory and fanning out at the level of the posterior STS to reach through the AG the posterior border of the occipital lobe. In 70% of the studied hemispheres (14/20), the MdLF reached the superior third of the posterior border of the occipital lobe; while in 30%, we also observed termination fibers at the middle third. Following the posterior retraction of the 3 segments of the MdLF, the fibers of UF, IFOF and ILF can be identified (Step 7) (Fig. 6).

Trajectory and morphology of the MdLF

The MdLF was invariably identified and recorded as a white matter bundle travelling under the U-fibers of the anterior STG/STS area and medial to both the U-fibers and the SLF/AF complex at the posterior temporal lobe and IPL. It was documented to connect the STG to the SPL and parieto-occipital area, by passing through the transverse gyri, and the STG to the posterior border of the occipital lobe through the AG. Regarding its configuration, the MdLF exhibits an anterior narrow part that progressively fans out at the posterior temporal lobe to reach the different parietal and occipital areas (SPL/PrC, POA and the occipital lobe/cuneus). With respect to its trajectory, the MdLF was observed to follow an anterolateral to posteromedial direction, as it moves from a more superficial layer anteriorly (medial to the U fibers) to a deeper dissection plane posteriorly (medial to the SLF/AF and VOF complex). Interestingly, as the MdLF runs through the transverse gyri, it demonstrates a characteristic “S-shaped” configuration with two slight curves; a lateral curve facing posteriorly and a medial curve facing anteriorly. The fibers that do not enter the transverse gyri exhibit a horizontal configuration with a slightly inferior and medial trajectory.

Subcortical correlative anatomy of the MdLF

Before highlighting the spatial relationship of the MdLF with adjacent fiber pathways, we have to stress that in almost all cases, we were able to achieve a discrete cleavage plane of this tract. We could, therefore, properly dissect it away from neighboring white matter bundles, mark it with white stripes, follow and lift the fibers of the different subcomponents from their origin to their termination points (Figs. 5, 6 and 7). The specific plane of latero-medial dissection and the distinct axonal connectivity of the discrete segments of the MdLF differentiate it from all the other fiber tracts that travel in the vicinity such as the SLF/AF complex, ILF, IFOF, UF, claustroradiation and external capsule radiations.

MdLF and SLF/AF complex We consistently identified the fibers of the MdLF to course just medial to the SLF/AF complex at the area of the parietal and occipital lobe. A

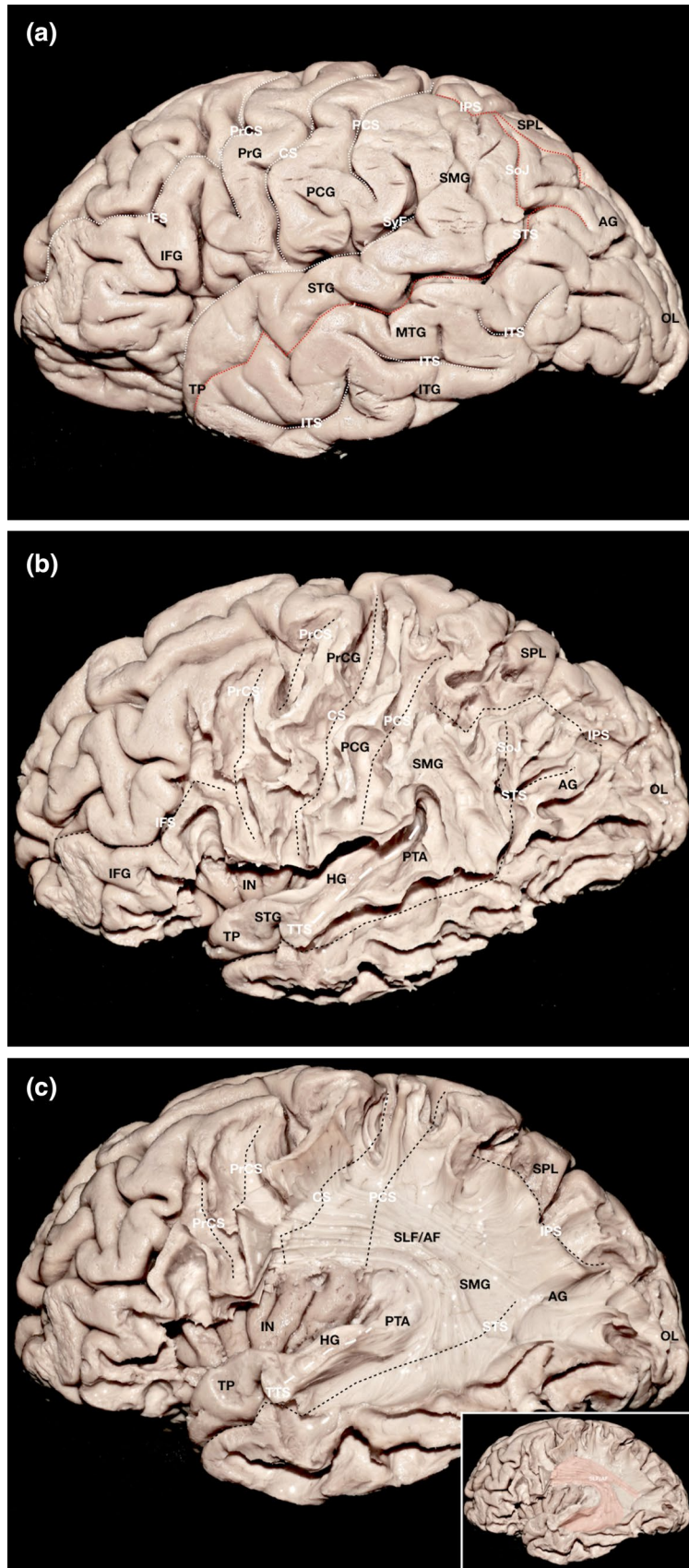


Fig. 2 Cortical and superficial subcortical anatomy. **a** Sulcal and Gyral anatomy of the lateral surface of a left hemisphere. The STS (demarcating the STG and the MTG), IPS (demarcating the SPL and the IPL) and SoJ (demarcating the SMG and AG) are marked with red dotted lines. The illustrated sulci of the lateral surface are marked with white dotted lines. **b** Same specimen with the U-fibers revealed (Step 1). The plane of the exposed sulci is outlined with black dashed lines for orientation purposes. Emphasis is placed on the anatomy of the STG and transverse gyri. The anterior transverse gyrus or Heschl's gyrus is demarcated from the posterior transverse area, which is defined as the remaining posteriorly placed transverse gyri (1–3), with the Transverse Temporal Sulcus (depicted using white bold dashed line). **c** Same specimen illustrating the SLF/AF complex (Step 2). The U-fibers of the inferior central lobe, IPL and TPO junction have been dissected and the SLF/AF complex, connecting the IFG, MFG and central lobe with the IPL and temporal lobe is illustrated. The inner fibers of the “C” shaped part of the SLF/AF complex terminating at the STG and STS should be removed with caution in order to preserve the underlying MdLF fibers. The Transverse Temporal Sulcus plane is depicted using a white bold dashed line, while the rest of the sulci with black dashed lines. Inset: the SLF/AF complex highlighted in red. *AG* angular gyrus, *CS* central sulcus, *HG* Heschl's gyrus, *IFG* inferior frontal gyrus, *IFS* inferior frontal sulcus, *IN* insula, *IPS* intraparietal sulcus, *ITG* inferior temporal gyrus, *ITS* inferior temporal sulcus, *MTG* middle temporal gyrus, *OL* occipital lobe, *PCG* postcentral gyrus, *PCS* postcentral sulcus, *PrCS* precentral sulcus, *PrG* precentral gyrus, *PTA* posterior transverse area, SLF/AF Superior Longitudinal Fasciculus/Arcuate Fasciculus Complex, *SMG* supramarginal gyrus, *SoJ* sulcus of Jensen, *SPL* superior parietal lobule, *STG* superior temporal gyrus, *STS* superior temporal sulcus, *SyF* sylvian fissure, *TP* temporal pole, *TTS* transverse temporal sulcus

tight anatomical proximity was observed between the fibers of the MdLF residing in the posterior transverse area and the most medial fibers of the “C”-shaped AF at the level of the STG. We, therefore, focused our dissection at the temporo-parietal junction and consistently developed a cleavage plane between the arching fibers of the AF and the more medially located fibers of the MdLF, which were seen to course towards the SPL and POA (Figs. 2c, 3a, b).

MdLF and dorsal external capsule Although the MdLF fibers that reside in Heschl's gyrus and the Dorsal External Capsule share the same direction and trajectory, there is nevertheless a clear cleavage plane between them. The MdLF courses more superficially and posteriorly in relation to the dorsal external capsule, while their respective anterior terminations are identified to exhibit a completely different and distinct pattern. More specifically, the fibers of the dorsal external capsule are seen to terminate in the area of the claustrum while the fibers of the MdLF are documented to end to the STG (Fig. 3b)

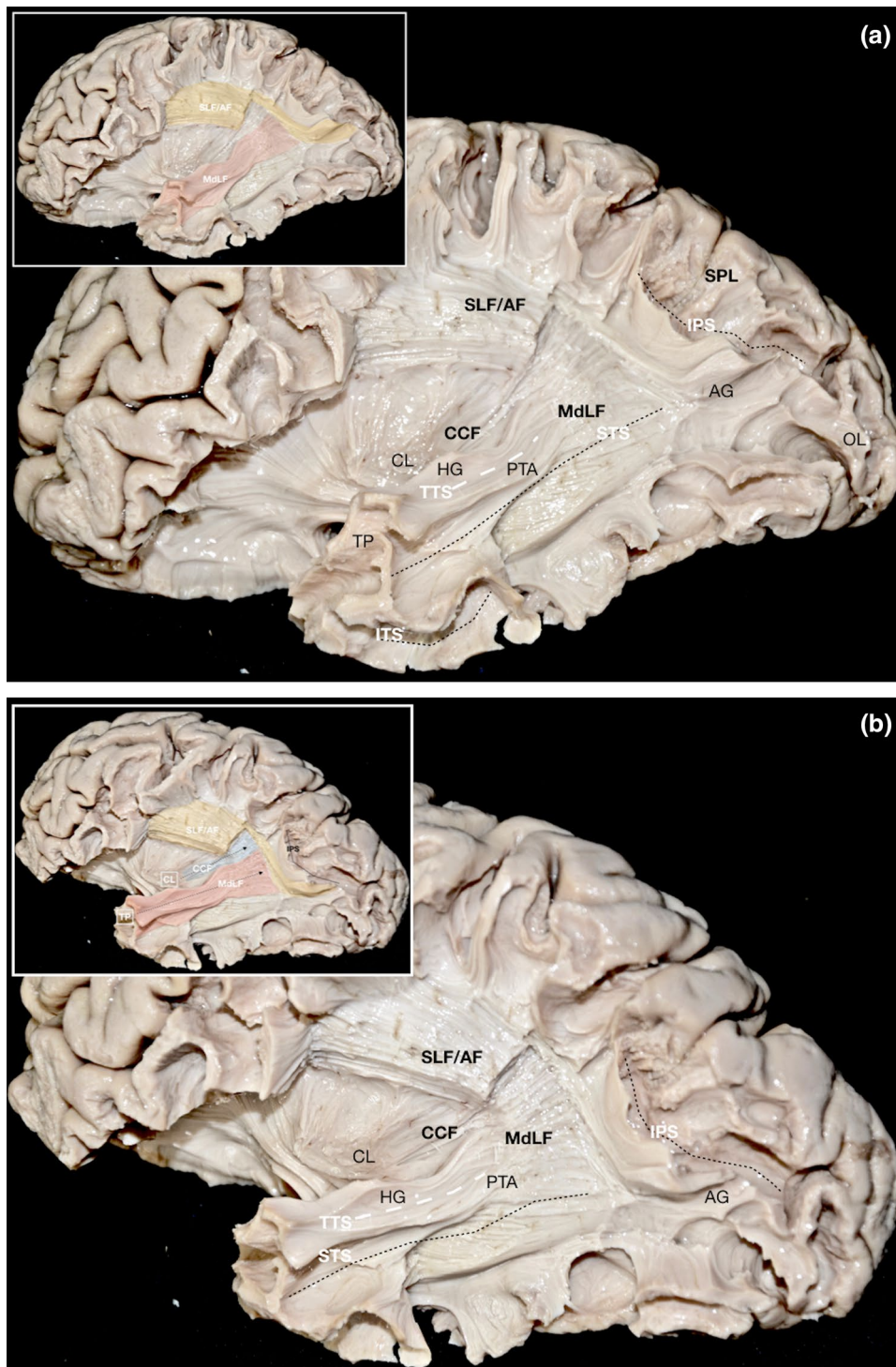
MdLF and UF Deep to the anterior part of the STG, fibers of the UF and MdLF were found to course in proximity. However, we observed the UF to lie medially to the MdLF at the anterior temporal lobe and to terminate more anteriorly in the temporal pole (Figs. 4b, 7d).

MdLF and IFOF We consistently recorded the IFOF to course in a deeper dissection plane than the MdLF, as its fibers dive towards the limen insula to reach the frontal lobe, thus corresponding to the ventral external capsule; whereas, the MdLF was seen to lie in a more superficial plane, medially to the U-fibers of the anterior STG–STS. Moreover, as the tracts travel posteriorly towards the occipital lobe, both the IFOF and MdLF merge with the sagittal stratum following, however, a distinct course; the MdLF runs dorsolaterally, while the IFOF exhibits a medial trajectory (Figs. 4c, 6c).

MdLF and ILF The ILF connects the TP to the occipital region, with its main stem travelling deep in the fusiform gyrus. Starting from the TP and focusing on their anterior correlative topography, the MdLF originates from the dorsal TP, while the ILF from the ventral TP (Figs. 6c, 7a, b). More specifically, the most inferior fibers of the MdLF are apparent at the level of the STS (Fig. 7c), while the stem of the ILF is located below the level of the ITS with its most superior fibers at the level of the middle temporal gyrus but always terminating more anteriorly and caudally in the TP, when compared to the MdLF fibers (Fig. 7a, b). At a deeper subcortical level, we recorded the anterior terminations of the MdLF to lie superior and posterior to the Uncinate Fasciculus fibers, while the ILF lying inferior to them (Fig. 7d, e). Again, the ILF fibers terminate distinctly more anteriorly in the temporal pole (Fig. 7d, e). Importantly, the ILF fibers turn towards the medial TP at the most anterior aspect of the tract (Fig. 7b, e). Tilting our dissection posteriorly, we consistently observed the fibers of the ILF to course and terminate in an inferior plane with respect to the MdLF (Fig. 7a, d, e). However, as they approach the posteriormost aspect of the occipital lobe and during their course in the sagittal stratum, the most superior ILF fibers seem to share occipital cortical terminations with the most inferior of the MdLF fibers in most of the cases (Fig. 7b).

Segmentation and connectivity pattern

After dissecting, detaching and retracting posteriorly the fibers of the MdLF, we consistently identified and recorded a specific connectivity and segmentation pattern. More specifically, fibers that originate from the dorsolateral TP were seen to enter the transverse gyri and to reach the SPL/PrC and POA, while the fibers originating more anterior and inferior (anteriormost part of STS and TP) were never encountered to pass through the transverse gyri. Instead, they course in a more medial and inferior trajectory, exhibiting a horizontal configuration and finally reaching the occipital lobe (Fig. 5). Three segments and connectivity patterns were invariably recorded. In line with previous white matter anatomy studies where the subcomponents of a full



bundle have been described [i.e., SLF; (Kamali et al. 2014; Makris et al. 2005; Martino et al. 2013; Petrides and Pandya 1984)], we used a similar nomenclature and we defined the three MdLF segments as MdLF-I, MdLF-II and MdLF-III.

MdLF-I: Dorsolateral TP and STG–Heschl’s gyrus–SPL/Pre-cuneus The MdLF fibers that travel through the anterior

transverse gyrus (Heschl’s Gyrus), exhibit an “S-shaped” configuration and terminate at the postero-superior SPL (Fig. 5b). These fibers reside more anteriorly and superiorly than the MdLF fibers entering the Posterior Transverse Area and also exhibit a superior trajectory towards the SPL (Fig. 5a). This segment travels parallel and posterolateral in

Fig. 3 Relationship between the MdLF and the IPL. Correlative anatomy with respect to the SLF and CCF (Step 3). **a** Same specimen as in Fig. 2. The temporal part of the MdLF is found under the fibers of the SLF/AF complex. The majority of the MdLF fibers were seen to enter the transverse gyri and course upwards and posteriorly, just medial to the SLF/AF complex. The U-fibers of the insula are dissected in order to expose the claustrum, delineate the claustralcortical fibers of the dorsal external capsule and distinguish them from the MdLF. The U-fibers of the IPS and TPO junction are preserved to illustrate the MdLF relationship with the IPL. Inset: the MdLF is highlighted in red and the remaining SLF/AF complex fibers in yellow. **b** Superolateral view of the same specimen. MdLF fibers and CCF fibers of the dorsal external capsule are illustrated. The MdLF lies postero-laterally with respect to the dorsal external capsule. The fibers of the MdLF can be tracked down to the TP; while those of dorsal external capsule are followed up to the claustrum. The MdLF passes deep to the IPS and continues towards the SPL and occipital lobe. The transverse temporal sulcus plane is depicted using white bold dashed line, while the rest of the exposed sulci using black dashed lines. Inset: The MdLF, SLF/AF complex and CCF are highlighted in red, yellow and blue, respectively. *AG* angular gyrus, *CCF* claustralcortical fibers, *CL* claustrum, *HG* Heschl's gyrus, *IPS* intraparietal sulcus, *ITS* inferior temporal sulcus, *MdLF* middle longitudinal fasciculus, *OL* occipital lobe, *PTA* posterior transverse area, *SLF/AF* superior longitudinal fasciculus/arcuate fasciculus complex, *SPL* superior parietal lobule, *STS* superior temporal sulcus, *TP* temporal pole, *TTS* transverse temporal sulcus

relation to the claustralcortical fibers of the dorsal external capsule (Fig. 3b).

MdLF-II: Dorsolateral TP and STG–Posterior transverse area–SMG–POA The MdLF fibers that originate at the dorsolateral TP and travel through the Posterior Transverse Area were seen to course obliquely and deep to the SMG. More specifically, they were always seen to terminate in a “U-shaped” configuration as a subcortical loop of fibers folding around the parieto-occipital sulcus, namely the parieto-occipital arcus (POA) (Fig. 5a, c). The MdLF-II lies more posteriorly, inferiorly and medially when compared to the MdLF-I and in an oblique and posteriorly directed course (Fig. 5a).

MdLF-III: most anterior part of TP/STS and STG–AG–occipital lobe/cuneus The MdLF fibers that stem from the most anterior part of the temporal pole and STS were consistently recorded to course in a relatively deep and inferior trajectory at the level of the STS. This segment exhibits a horizontal configuration and fans out at the level of the posterior STS to reach the posterior border of the occipital lobe and cuneus by passing deep to the AG (Figs. 5a, d, 7). It joins the sagittal stratum as its most dorsolateral part. In 70% of the hemispheres, this segment was seen to terminate at the superior third of the posterior lip of the occipital lobe, while in 30% we also observed termination fibers in the middle third (Fig. 6b).

DTI imaging

The applied multi-ROI tractography protocol was successful for the reconstruction of the entire MdLF. The trajectory and morphology of the reconstructed MdLF were in line with the fibers identified during the white matter fiber dissection part of the study, based on which we further applied a multi-ROI tractography protocol to verify the existence of sub-segments. Specifically, for the reconstruction of segments I–III of the MdLF, three ROIs on the coronal plane were also used based on the termination pattern identified during the dissection component of the study. The first two ROIs at the level of the superior temporal gyrus were the same as the ones used for the entire MdLF. For the third ROI (Fig. 8), the mid-part of parieto-occipital sulcus was clearly identified in the sagittal plane and a ROI was placed in the coronal plane based on discrete anatomical boundaries (Petrides 2012) covering: (a) the superior parietal lobule (SPL)/precuneus (PrC) (MdLF-I); (b) a medial region of the hemisphere between the precuneal sulcus, the paroccipital segment of the intraparietal sulcus and posterior calcarine sulcus (MdLF-II); (c) and the anatomical area lateral to the paroccipital segment of the intraparietal sulcus and inferior to the posterior calcarine sulcus (MdLF-III). Exclusion ROIs were used in case of erroneous fibers.

To better clarify the termination pattern of MdLF, each reconstructed MdLF for the left and the right hemispheres were colour-coded based on the FA and superimposed on each subject anatomical T1. Lower values (close to 0.1) at the edges of each fiber are indicative of low FA close to the cortical termination on gray matter (Fig. 9). The trajectory of the entire MdLF on coronal and axial (Fig. 10) for a single subject is superimposed on subject's T1 image. The main trajectory of the MdLF (entire bundle) was similar in all subjects with the main stem passing along the STG, although there was some variation in the course of the fibers, specifically at the most posterior part of bundle. Caudally, at the TPO transition area of STG, the three segments of the MdLF fan out to reach the parietal and occipital areas, in line with the dissection data. The trajectory of the MdLF segments on coronal (Fig. 11), axial (Fig. 12) and sagittal (Fig. 13) plane is superimposed on anatomical T1 for a representative subject. MdLF-I courses dorsally to MdLF-II and MdLF-III and medially to MdLF-III segment. The MdLF-II is located medially to MdLF-III, ventrally to the MdLF-I and dorsally to the MdLF-III fibers, which terminate at the lateral and inferior occipital cortex. MdLF-III is the most laterally situated segment.

Concerning the trajectory and the terminating fibers of MdLF segments, both MdLF-I and MdLF-II had a relatively homogeneous pattern, terminating in the SPL/PrC and POA, respectively. On the other hand, the pattern of the terminating fibers of MdLF-III varied between the subjects, although

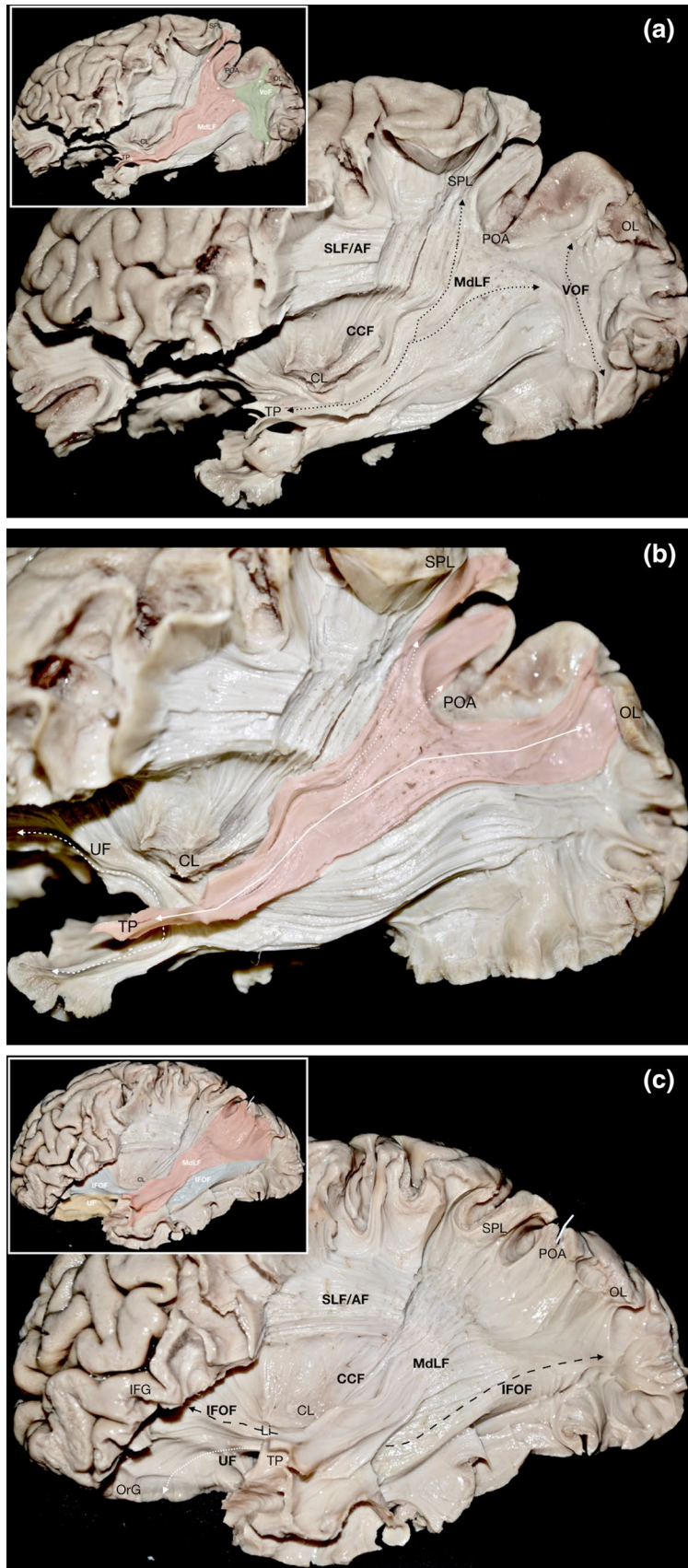


Fig. 4 Illustration of the temporo-parietal and temporo-occipital connections of the MdLF. **a** Different specimen. Left lateral side. The MdLF temporo-parietal connection is delineated (Step 4) extending up to the postero-superior part of the SPL/PrC and the parieto-occipital area. Dissecting away the U-fibers of the TPO junction exposes fibers of the MdLF continuing posteriorly to enter the occipital lobe. The VOF, running under the U-fibers of the occipital lobe and exhibiting a vertical trajectory can be also identified. Inset: the MdLF is highlighted in red and the VOF in Green. The trajectories of the MdLF and VOF are outlined with black dotted arrows. **b** Same specimen as in (a). Following dissection of the VOF, the MdLF temporo-occipital connection reaching the posterior border of the occipital lobe/cuneus is illustrated (Step 5). The silhouette of the MdLF is highlighted in red. The temporo-occipital connection is indicated with the white arrow and the temporo-parietal connection with the white dotted arrows. The UF is outlined with white dashed arrowed line. The UF lies medially to the MdLF at the anterior temporal lobe and terminates more anteriorly and inferiorly in the temporal pole. **c** Same specimen as in Fig. 2. Relationship between the MdLF, IFOF and UF. The MdLF is seen to reach the anterior part of the STG and the TP. It is also clearly distinguished from the UF and IFOF, which travel in a deeper dissection plane as they form the ventral external capsule at the level of limen insula. The trajectory of the IFOF is demonstrated with the black dashed arrow as it courses ventromedial to the MdLF at the level of the temporal lobe and the sagittal stratum. The orbito-frontal part of the UF is depicted with the white dotted arrow. Inset: The MdLF, IFOF and UF are highlighted in red, blue and yellow, respectively. *CCF* claustrum-cortical fibers, *CL* claustrum, *IFG* inferior frontal gyrus, *IFOF* inferior fronto-occipital fasciculus, *Li* limen insula, *MdLF* middle longitudinal fasciculus, *OL* occipital lobe, *OrG* orbital gyri, *POA* parieto-occipital arcus, *SLF/AF* superior longitudinal fasciculus/arcuate fasciculus complex, *SPL* superior parietal lobule, *TP* temporal pole, *UF* uncinata fasciculus, *VOF* vertical occipital fasciculus

in all cases MdLF-III passed through the AG. More specifically, concerning the occipital lobe, fibers did not terminate in the inferior occipital cortex in 31.43% (left) and 11.43% (right) and in the lateral occipital cortex in 31.42% (left) and 17.14% (right) of MdLF-III cases. Figure 14 depicts the pattern of MdLF segments on a coronal plane for subject HPC_MGH_1031 where a similar pattern of MdLF-I and MdLF-II is found bilaterally in contrast to the trajectory of MdLF-III; MdLF-III fibers of the right hemisphere do not terminate on inferior occipital cortex but only on lateral occipital cortex. The S.I. for the entire MdLF and its segments for mean FA, AD and RD are presented for each subject in Table 1. No statistically significant left–right differences at $p < 0.05$ after correcting for multiple comparisons were identified. The group-wise quantitative DTI indices and coefficient of variation (CV%) are presented in Table 2. The variability of the reconstructed tracts for the left and right hemispheres for all participants is depicted by CV%.

With regard to the topography of the MdLF as compared to the adjacent tracts, the entire MdLF courses dorsally and laterally to the ILF (Fig. 15), laterally to the IFOF (Fig. 16) and UF (Fig. 17), and medially to the SLF (Fig. 18). The rostral part of the MdLF is located at the dorsal TP at the level of the STG, whereas the ILF courses mostly at the

level of middle and inferior temporal gyri. At the level of the STG, the inferior part of SLF is located laterally to the MdLF. The temporal extent of the UF is located medially and anteriorly to the rostral part of the MdLF. Considering the high proximity between MdLF and ILF and recent DTI studies concerning overlapping regions between the two tracts (Bullock et al. 2019; Panesar et al. 2018), Supplementary Figs. 1–3 provide a more comprehensive visualization of the correlation anatomy between MdLF segments and ILF (Supplementary Fig. 1–3). As it is shown in supplementary figures, there is no clear overlap between the anterior termination fibers of MdLF segments and ILF which runs more anteriorly. At the posterior aspect within the occipital lobe, the MdLF-III shares termination areas with the ILF. However, the trajectory of the MdLF-III as it travels anteriorly and the validity of the tractography algorithm in case of crossing, kissing and/or licking fibers (Christidi et al. 2016; Karavasilis et al. 2019) enable an accurate reconstruction of this MdLF segment. To further clarify this issue, we have additionally reconstructed the corona radiata and optic radiation to showcase regions where fibers from MdLF, corona radiata and optic radiation are successfully reconstructed without the constraints of fiber crossing (Fig. 19).

Discussion

The first description of the MdLF in humans can be traced back to the recent past when Makris and colleagues provided novel radiological evidence on its existence and structure. The authors, by implementing a focused DTI protocol, supported the hypothesis that the MdLF represents a long cortico-cortical tract between the STG and AG (Makris et al. 2009). Subsequent anatomical and anatomo-tractographic studies, however, underpinned a wider and at times different connectivity pattern, by including various post-rolandic areas such as the SMG, SPL, PrC, occipital lobe, cuneus and have inevitably introduced ambiguity and controversy regarding the tract's inherent architecture (Table 3) (Conner et al. 2018; Makris et al. 2013a, b; Makris et al. 2017; Maldonado et al. 2013; Menjot de Champfleury et al. 2013; Tremblay et al. 2019; Wang et al. 2013). In this vein, although the main body of DTI data converge on the robust connectivity between the STG and AG (Makris et al. 2009, 2013a, b; Makris et al. 2017; Menjot de Champfleury et al. 2013; Tremblay et al. 2019), the two available anatomic reports suggest otherwise (Maldonado et al. 2013; Wang et al. 2013). On a closer look, Maldonado and colleagues claim that the thus far prominent MdLF terminations to the AG and SMG were not identified, while Wang and colleagues have demonstrated very few fibers terminating to the IPL. Further, Maldonado describes the MdLF largely as a temporo-occipital tract with no parietal connections, while Wang on the

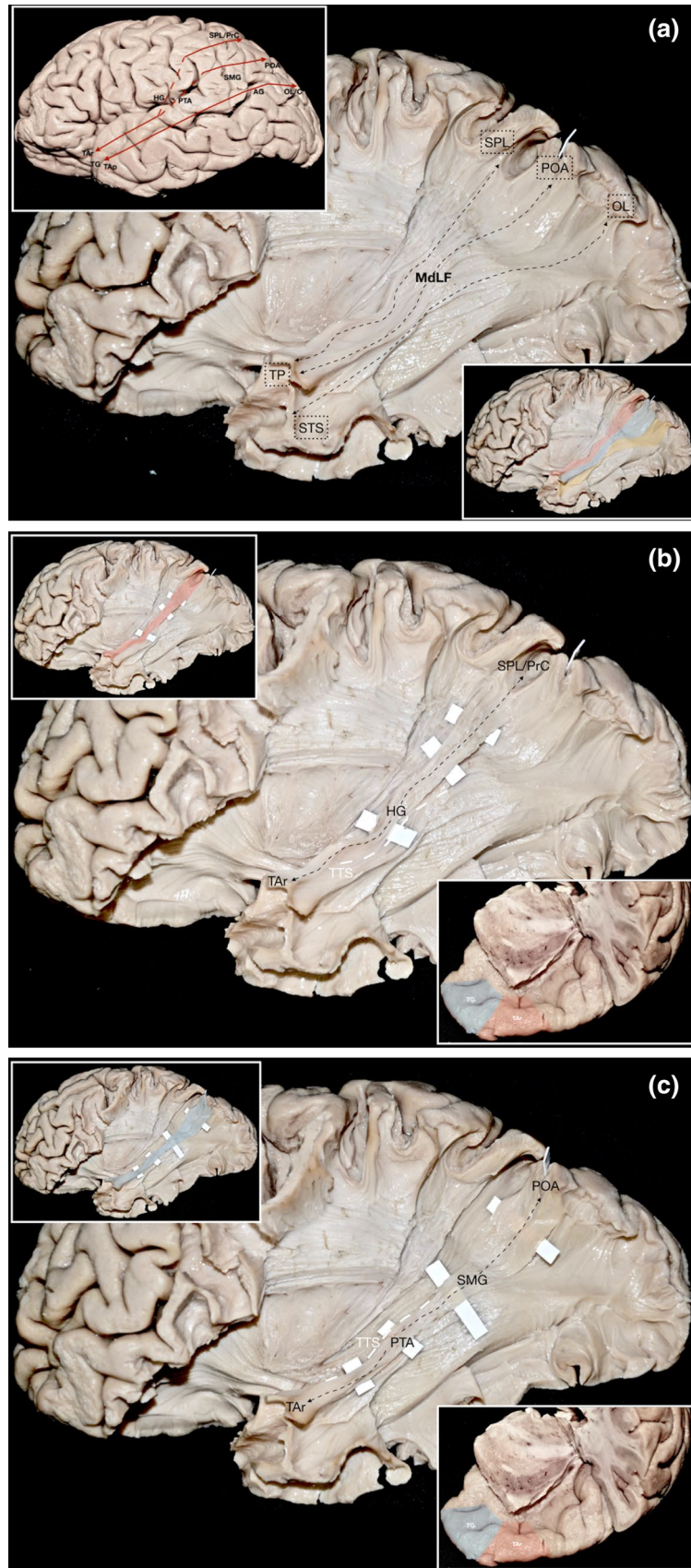


Fig. 5 Connectivity and segmentation pattern (Step 6). **a** Left hemisphere—Same as in Fig. 2. The MdLF is consistently recorded to connect various segments of the TP and STG with the SPL/PrC, POA and occipital lobe/cuneus, by passing through the transverse gyri and the IPL (SMG and AG). The fibers originating at the dorsolateral TP were seen to travel through the transverse gyri to reach the SPL and the parieto-occipital arcus (MdLF-I and MdLF-II). The fibers originating at the anteriormost STS and TP, reach the occipital lobe/cuneus (MdLF-III) without travelling through the transverse gyri. Upper inset: Connectivity and terminations of the MdLF (red line and arrows) superimposed on the superficial anatomy, Lower inset: Trajectory and terminations of the three segments of the MdLF; MdLF-I, MdLF-II and MdLF-III highlighted in red, blue and yellow, respectively. **b** Same specimen, Hyper-Selective dissection of the fibers of the MdLF-I. MdLF fibers that originate from the dorsolateral TP, corresponding to the area TAr, enter the Heschl's Gyrus (anterior to the plane of Transverse Temporal Sulcus) and follow a superior trajectory to terminate at the supero-posterior part of the SPL/PrC. The trajectory and connectivity of MdLF is marked with the black dashed arrow. Upper inset: The MdLF-I highlighted in red. Lower inset: a superolateral view of the exposed dorsal TP and superior STG on a left hemisphere, after cutting through the temporal stem and disconnecting the frontal lobe. The TG and TAr areas are highlighted in blue and red, respectively. Note the axial cut on the central core. **c** Same specimen as above, Hyper-selective dissection of the MdLF-II. The MdLF-I has been carefully removed and the trajectory and connectivity of the MdLF-II is vividly illustrated. MdLF fibers originating from the dorsolateral TP, corresponding to the area TAr, are seen to travel through the posterior transverse area (posterior to the plane of transverse temporal sulcus) and to course obliquely in the depths of SMG, finally reaching the parieto-occipital arcus, i.e., the area folding around the parieto-occipital sulcus. Upper inset: The MdLF-II highlighted in blue. Lower inset: The TG and TAr areas highlighted in blue and red, respectively. **d** Same specimen, Hyper-selective dissection of the MdLF-III. The MdLF-I and MdLF-II have been removed and the fibers of the MdLF-III are revealed. The MdLF-III consists of fibers originating at the most anterior part of the TP and STS, which correspond to the areas TG and TAp, respectively. These fibers travel in the depth of the STS, pass under the AG and reach the posterior border of the occipital lobe/cuneus. Upper inset: The MdLF-III highlighted in yellow. Lower inset: an antero-inferior view of the TP of the same left hemisphere highlighting the areas TG, TAr and TAp in blue, red and yellow, respectively. *AG* angular gyrus, *C* cuneus, *HG* Heschl's gyrus, *MdLF* middle longitudinal fasciculus, *OL* occipital lobe, *POA* parieto-occipital arcus, *PrC* precuneus, *PTA* posterior transverse area, *SMG* supramarginal gyrus, *SPL* superior parietal lobule, *STS* superior temporal sulcus, *TP* temporal pole, *TTS* transverse temporal sulcus

contrary emphasizes on the tract's dissemination to the SPL and PrC (Maldonado et al. 2013; Wang et al. 2013).

Hence, to clarify the MdLF connectivity pattern, we meticulously investigated all the previously described putative connections of the STG and TP through a focused anatomico-imaging protocol. Indeed, we identified and recorded a tight anatomical relationship with all the aforementioned areas. However, although we have consistently demonstrated the MdLF to pass deep to the IPL (AG and SMG), we did not isolate any significant cortical terminations to the SMG and AG, therefore agreeing with previous anatomical and anatomico-tractographic studies (Maldonado

et al. 2013; Wang et al. 2013). The theory that the SMG–AG complex is as a principal MdLF termination area, advocated by the majority of DTI studies, is in our view susceptible to the inherent limitations of this technique, which are mainly attributed to the crossing, kissing and bending effects of adjacent white matter fibers and which consequently decrease the anatomical accuracy of this method (Fernandez-Miranda et al. 2012; Johansen-Berg and Rushworth 2009; Le Bihan et al. 2006; Oouchi et al. 2007; Vos et al. 2011). In this regard, the presence of a sizable SLF/AF complex located in a superficial plane to the MdLF in the area of the IPL (Gungor et al. 2017; Koutsarnakis et al. 2015) and exhibiting abundant fibers radiating towards the IPS and AG (Monroy-Sosa et al. 2019) lends support to the notion that the hypothetical MdLF fibers terminating to the AG and identified as such by DTI studies are in essence SLF/AF fibers (Fig. 3). On the contrary, the potential MdLF connections to the SPL, PrC, occipital lobe and cuneus can be readily and consistently identified thus proving that this bundle is both a temporo-parietal and temporo-occipital white matter pathway (Figs. 4, 5). Importantly, the qualitative comparison of our dissection and tractography results provides evidence of similar findings concerning the anatomical trajectory of the entire MdLF and its topography in relation to adjacent white matter tracts (i.e. ILF, IFOF, UF, SLF).

Finally, a lack of agreement on whether the MdLF reaches the TP or not can be traced throughout the relevant literature. Although the majority of the available DTI evidence points positively towards this direction (Makris et al. 2013a, b; 2017; Menjot de Champfleury et al. 2013; Tremblay et al. 2019), the study by Conner and colleagues places the MdLF further posteriorly along the temporal lobe (Conner et al. 2018). Ambiguity remains even in the two published anatomical reports, with Maldonado et al. not reaching a safe conclusion on this issue; while, Wang and colleagues on the contrary advocate that only the deep and long subcomponent of the MdLF, which terminates at the occipital lobe, reaches the temporal pole (Maldonado et al. 2013; Wang et al. 2013). In this study, we have vividly demonstrated and consistently recorded all three segments of the MdLF to terminate in different areas of the TP (Fig. 4, 5). Recently, Ding and colleagues parcellated the human temporo-polar cortex into specific sub-regions using cytoarchitectonic and chemoarchitectonic methods as well as pathological markers (Ding et al. 2009). According to the authors, the area TAr is located at the dorsolateral TP, anterior to the typical TA area or parabelt auditory cortex, the area TAp is located at the dorsal bank of the anterior superior temporal sulcus, and the area TG is a dysgranular region of the most anterior part of the TP, occupying to some extent the dorsal aspect of the TP (Fig. 5). Our results, therefore, suggest that the anterior terminations of the MdLF-I and II reside at the TAr area

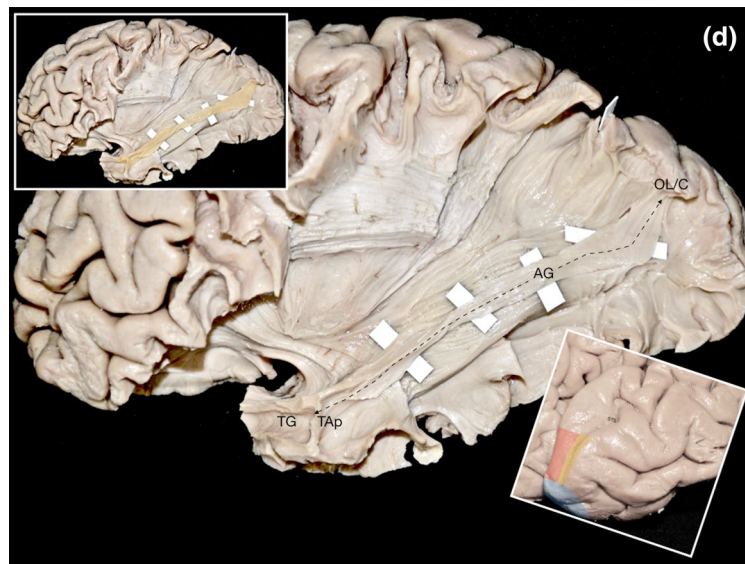


Fig. 5 (continued)

(Fig. 5a–c), while those of the MdLF-III correspond to the areas TG and TAp (Ding et al. 2009) (Fig. 6a, d).

Functional considerations and segmentation pattern of the MdLF

Early theories have hypothesized that the MdLF is a component of the language pathway (Makris and Pandya 2009; Makris et al. 2009). This hypothesis was largely based on its connectivity pattern which involved language-specific areas such as the STG and IPL; More specifically, on the basis of contemporary speech processing models (Gow Jr et al. 2008; Hickok and Poeppel 2007), it has been advocated that the STG–AG MdLF connection is implicated in translating phonemes into articulatory forms, while the STG–SMG connection subserves phonetic processing (Makris et al. 2017). Regarding the non-dominant hemisphere, the MdLF has been associated with visuospatial processing due to its parietal connections (Galati et al. 2001; Galletti and Fattori 2002; Macaluso et al. 2003). Beyond language and visuospatial functions, the MdLF has been also linked to the integration of higher order auditory and audiovisual functions (Makris et al. 2013b, 2017; Wang et al. 2013) with very recent findings strongly implicating this tract in speech perception and auditory processing ability in noise (Tremblay et al. 2019) (Table 3).

In line with our results, evidence from previous anatomical (Maldonado et al. 2013) and anatomo-tractographic studies (Wang et al. 2013) have supported the lack of a rich connectivity between the STG and the IPL (Geschwind’s area) through the MdLF. In addition, direct cortical stimulation of the dominant MdLF in 8 patients during awake craniotomies

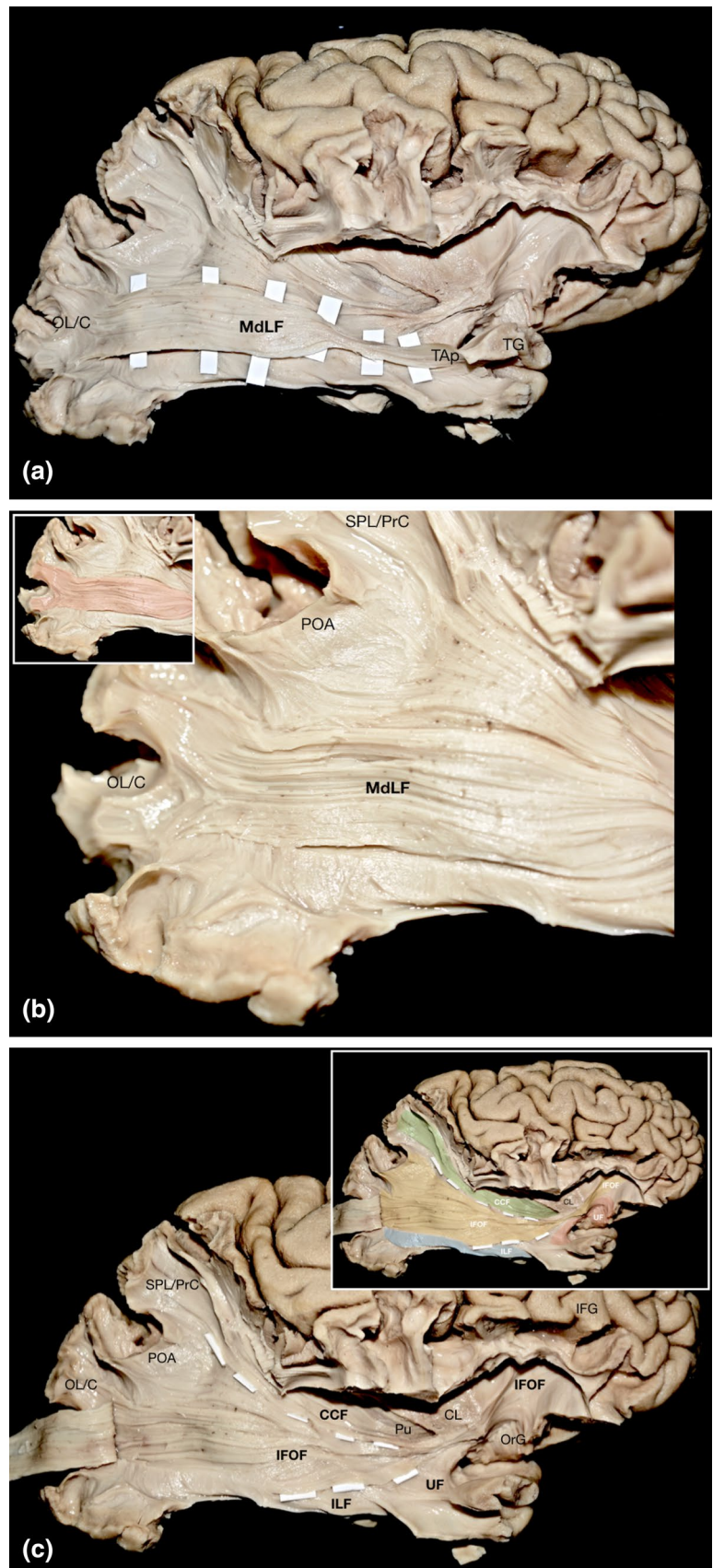
revealed no language interference during picture-naming tasks, while the detailed postoperative language assessment following surgical resection of brain regions including the MdLF showed no permanent speech-related deficits (De Witt Hamer et al. 2011).

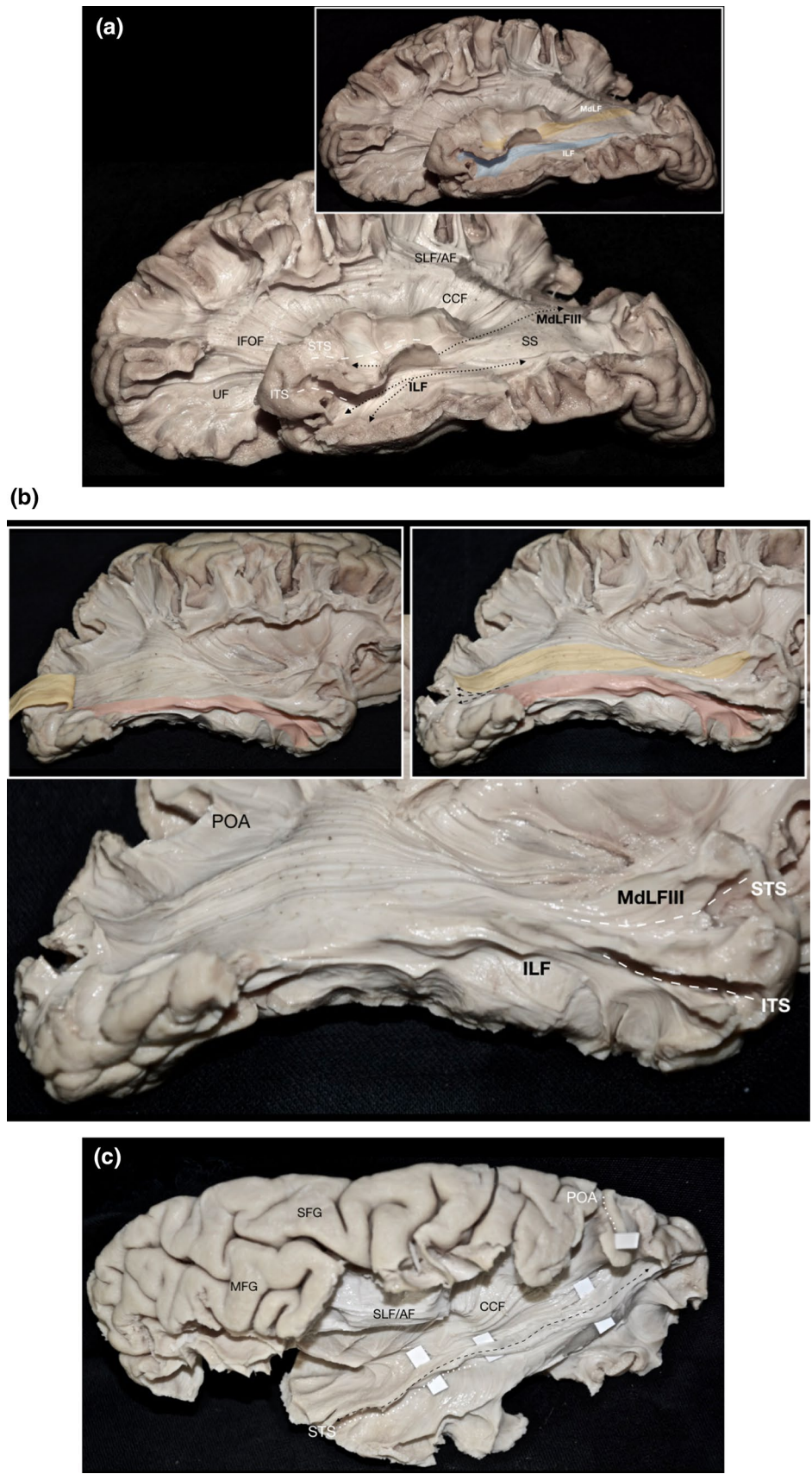
However, the intraoperative stimulation and the surgical resections included only the anterior part of the MdLF and therefore, no insights were gathered with respect to the function of the posterior part of the tract. Furthermore, a statistically significant leftward lateralization of the MdLF was not disclosed, in terms of descriptive DTI measures such as volume and FA, by previous (Makris et al. 2009b 2013a b; Wang et al. 2013) and the present study. Conversely, it has been well documented that tracts crucial for language, such as the AF (Matsumoto et al. 2008) and SLF (Makris et al. 2004), exhibit considerable asymmetry in terms of volume and FA, according to language lateralization (Catani et al. 2007). All the above tend to shift the paradigm of the MdLF away from language functions.

In our study, a tight anatomical relationship between the MdLF and the transverse gyri, i.e., the primary and secondary auditory cortices, has been invariably recorded both in white matter dissections and in vivo tractography (Fig. 3). We have, thus, demonstrated the MdLF-I to course always through the anterior transverse gyrus (Heschl’s Gyrus) (Fig. 5b) and the MdLF-II to travel just under the cortex of the posterior transverse gyri/posterior transverse area (Fig. 5c). Further, the observation that the MdLF proves to be the most prominent white matter pathway of the transverse gyri provides a sound structural basis for its alleged functional implication in auditory processing (Howard et al. 1996, 2000; Lewald and Getzmann 2011; Liegeois-Chauvel

Fig. 6 MdLF Occipital terminations and relationship with deeper fiber tracts (Step 7).

a Different specimen. Right lateral side. Hyper-selective dissection of the MdLF-III. **b** Focused view of the occipital area of the same specimen as in (a). Fibers of the MdLF-III are seen to terminate at the superior and middle third of the occipital lobe/cuneus. In 70% of the hemispheres studied (14/20), the MdLF was recorded to reach the superior third of the posterior border of the occipital lobe; while in the remaining 30%, termination fibers at the middle third were also detected. Inset: the MdLF-III highlighted in red. **c** Same specimen as in (a). Following the dissection and retraction of the MdLF-III (step 7) the fibers of UF, IFOF and ILF can be identified. The silhouette of the IFOF is depicted and demarcated from the CCF and UF with small white pads. The IFOF lies medial to the MdLF. The UF lies also medial to the MdLF at the anterior temporal lobe and terminates more anteriorly in the temporal pole as illustrated in the figure. In contrast to the MdLF, the fibers of the ILF are seen to originate from the ventral TP and to course in an inferior plane with respect to the MdLF, however sharing some cortical terminations. Inset: The MdLF, IFOF, UF, CCF and ILF highlighted in red, yellow, orange, green and blue, respectively. *C* cuneus, *CCF* claustrum-cortical fibers, *CL* claustrum, *IFG* inferior frontal gyrus, *IFOF* inferior fronto-occipital fasciculus, *ILF* inferior longitudinal fasciculus, *MdLF* middle longitudinal fasciculus, *OL* occipital lobe, *OrB* orbital gyri, *POA* parieto-occipital arcus, *PrC* precuneus, *Pu* putamen, *SPL* superior parietal lobule, *UF* uncinate fasciculus





◀ **Fig. 7** MdLF-III correlative anatomy with respect to ILF at the sulcal and deep subcortical levels. **a** Different specimen. Left hemisphere. Inferolateral view. The levels of the STS and ITS are outlined with dashed white lines. The MdLF-III is seen terminating anteriorly at the level of the STS and dorsal TP, while the ILF anterior terminations are being recorded at the level of ITS and ventral TP. Inset: The MdLF-III and ILF highlighted in yellow and blue, respectively. **b** Same specimen as in Fig. 6. Right hemisphere. Inferolateral view. Again, MdLF-III and ILF anterior terminations at the level of the STS and ITS/ventral TP, respectively. ILF fibers are seen turning towards the medial TP at the most anterior aspect of the tract. Posteriorly both tracts merge with the sagittal stratum and share occipital cortical terminations. Insets: MdLF-III and ILF are highlighted in yellow and red, respectively. In the right inset, their shared occipital cortical terminations are outlined with black dashed arrowed lines. In the left inset, the MdLF-III has been retracted posteriorly. **c** Different Specimen. Left hemisphere. Superior view. The STS and POA are outlined with white dotted lines. MdLF-III is demarcated with small white pads and outlined with a black dashed arrowed line. The MdLF-III is seen as a distinct white matter tract, coursing at the level of STS towards the occipital lobe. Residual U-fibers of the STS delineate MdLF-III from other long white matter tracts in vicinity including ILF. **d** Same specimen as in Fig. 4a. Left hemisphere. Lateral view. MdLF-III is dissected away from neighboring tracts and demarcated with small white pads. ILF is highlighted in blue. UF is outlined with black dashed arrowed line. The anterior terminations of the MdLF lie superior and posterior to the uncinete fasciculus fibers, while the ILF lying inferior to them. The ILF fibers terminate distinctly more anteriorly in the temporal pole. IFOF is outlined with black dotted arrowed line. MdLF-I and -II have been retracted posteriorly and highlighted with yellow and red, respectively. **e** Same specimen as in Fig. 4a. Left Hemisphere. Inferolateral view. The distinctly different anterior terminations of MdLF-III and ILF are apparent. The space between them is outlined with black dotted arrowed line. Again, the ILF is seen turning towards the medial TP. Right inset: MdLF-III and ILF are highlighted in green and blue, respectively. Left inset: MdLF-I, -II (retracted posteriorly) and -III are highlighted in yellow, red and green, respectively, while the ILF is outlined with dashed arrowed lines. *CCF* claustrum-cortical Fibers, *CL*=claustrum, *IFOF* inferior fronto-occipital fasciculus, *ILF* inferior longitudinal fasciculus, *ITS* inferior temporal sulcus, *MdLF* middle longitudinal fasciculus, *MFG* middle frontal gyrus, *POA* parieto-occipital Arcus, *SFG* superior frontal gyrus, *SLF/AF* superior longitudinal fasciculus/arcuate fasciculus complex, *SS* sagittal stratum, *STS* superior temporal sulcus, *UF* uncinete fasciculus

et al. 1991). In that respect, although assumptions on the role of the MdLF in higher auditory processing have been previously made (Burks et al. 2017; Wang et al. 2013), none of the published studies has provided anatomical evidence on the structural correlation of the MdLF and its segments with the auditory cortex. The potential auditory role of the MdLF is additionally supported by novel functional data regarding specific subregions of the temporal pole to which the tract is seen to terminate. More specifically, we have demonstrated that the MdLF terminates at the dorsolateral TP and the most anterior part of the STS and TP, areas which correspond to the TAr, TAp and TG subregions, respectively (Ding et al. 2009) (Fig. 5). According to functional studies in

non-human primates, the area TAr (Fig. 5), i.e., the equivalent of the dorsolateral TP, has been implicated in high-order auditory processing (Hackett et al. 1999; Poremba et al. 2003; Romanski et al. 1999) with remarkable neural activities being detected following specific vocal calls (Poremba et al. 2004). Moreover, the area TAp, which equals the upper bank and fundus of the superior temporal sulcus, was documented to respond both to auditory and visual stimuli in non-human primates, and has, thus, been considered as a polysensory association cortex (Seltzer and Pandya 1978, 1991).

Functional literature focusing on auditory pathways and perception of sounds supports the hypothesis that non-primary auditory cortex located posterior to the Heschl's gyrus is involved in the spatial processing of sounds (Brunetti et al. 2005; Krumbholz et al. 2004; Tata and Ward 2005a, b; Warren et al. 2002; Zimmer and Macaluso 2005); while, areas in or anterior to Heschl's gyrus subserve the processing of phonetic stimuli (Binder et al. 2000; Obleser et al. 2006) and pitch characteristics (Warren and Griffiths 2003). Further, similar to the well-established dorsal and ventral visual streams, the existence of respective parallel auditory pathways is also advocated by field researchers (Lomber and Malhotra 2008; Rauschecker and Scott 2009; Rauschecker and Tian 2000; Tian et al. 2001). More specifically, Ahveninen and colleagues, using functional MRI (fMRI) and magnetoencephalography (MEG) in humans, demonstrated that the “what” auditory pathway, which is responsible for processing auditory object identity characteristics, stems from the anterior auditory cortex (anterolateral Heschl's gyrus, anterior STG and posterior Planum Polare); while, the “where” auditory pathway, which is responsible for processing the location characteristics of sound, stems from the posterior auditory cortex (posterior Planum Temporale and STG). Most importantly, they prove that the “where” pathway is activated significantly earlier than the “what” pathway, therefore aiding in auditory object appreciation through a top-down spatial information transmission (Ahveninen et al. 2006). In other words, the activation of the “where” pathway precedes to shift and maintain the attention towards the identity characteristics of the pertinent auditory object (Jääskeläinen et al. 2004).

Hence, in an effort to couple function to anatomy, it could well be argued that the MdLF-II, which is anatomically proved to connect the TAr area to the posterior auditory cortex and posterior parietal cortex, may resemble the posterior or “where” pathway; whereas the MdLF-I, which connects the parietal cortex to the anterior auditory cortex and TAr, could represent the anterior or “what” auditory pathway. Hypothetically, the MdLF-I and MdLF-II as

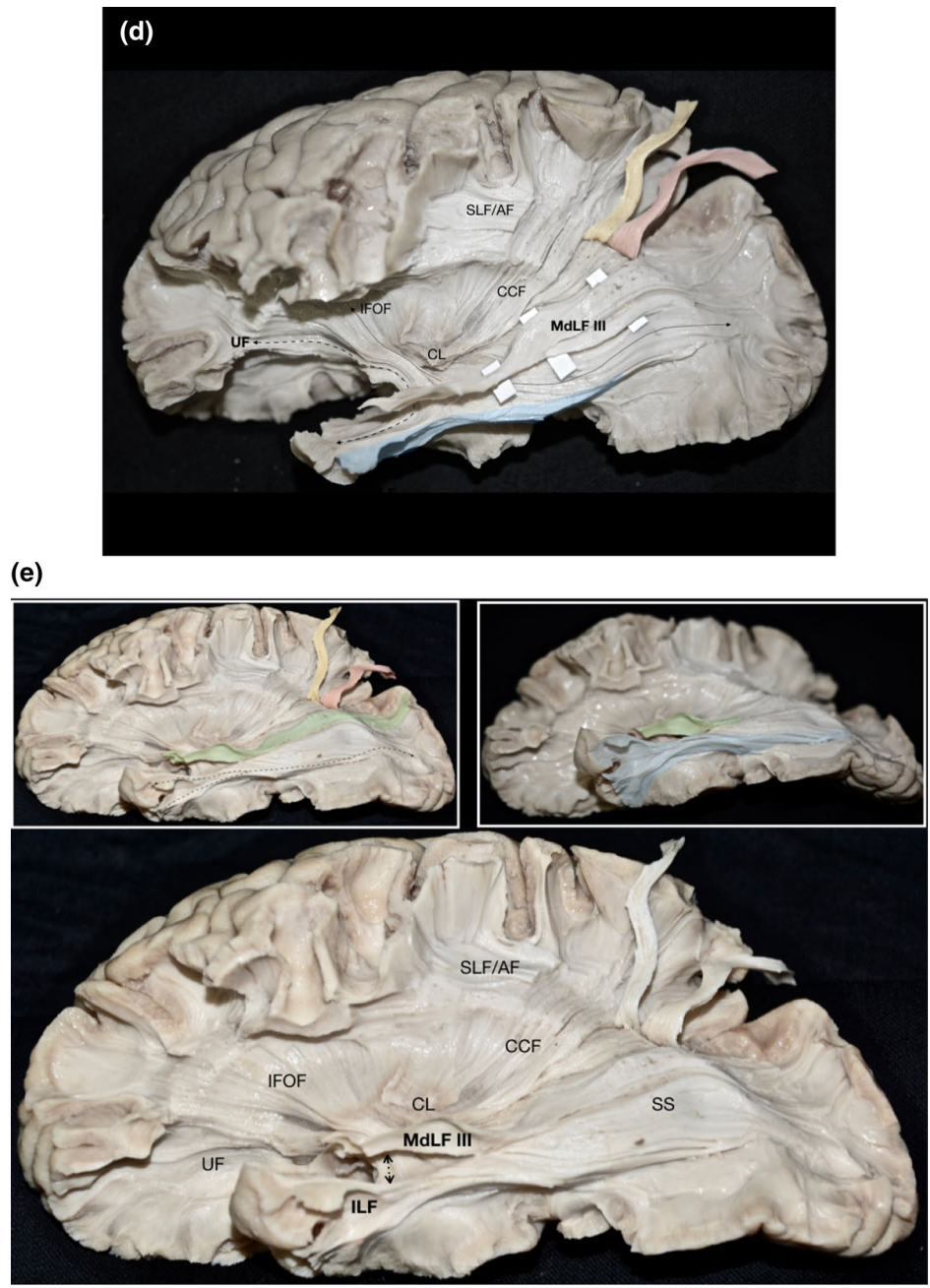


Fig. 7 (continued)

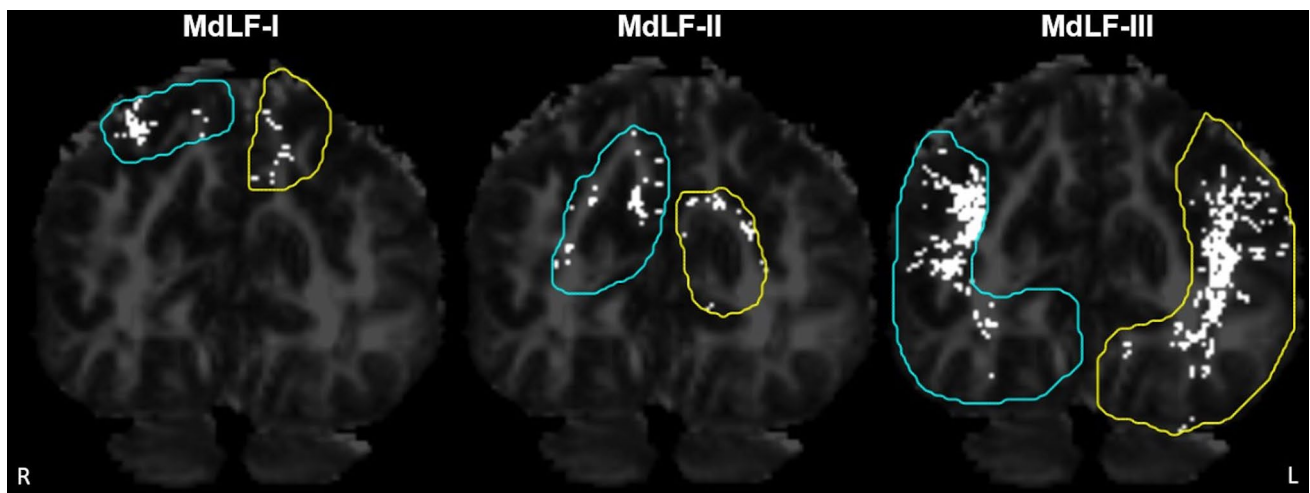


Fig. 8 Representation of the placement of the third ROI for the reconstruction of MdLF-I (left panel), MdLF-II (middle panel) and MdLF-III (right panel) segments in the left (colored in yellow) and the right (colored in cyan) hemisphere. ROIs are projected over an FA map in

coronal plane. The first two ROIs were the same as ROI 1 and ROI 2 used for the reconstruction of the entire MdLF. ROI region of interest, MdLF middle longitudinal fasciculus

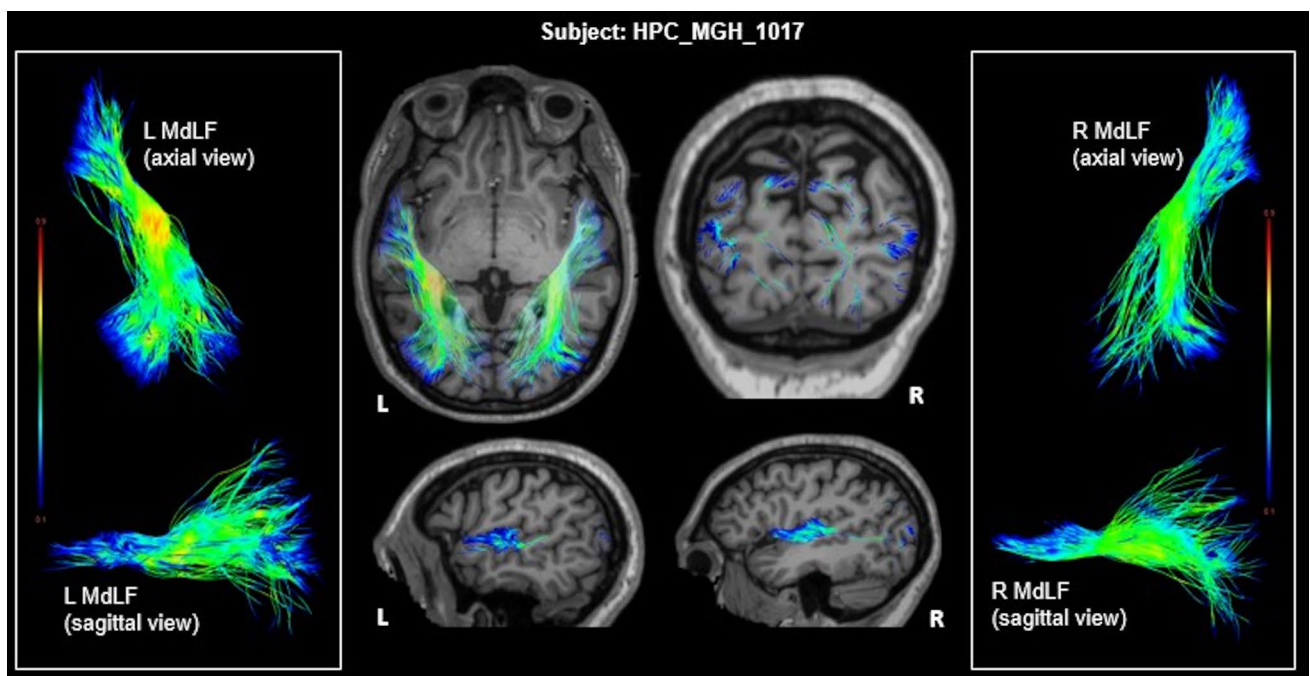


Fig. 9 Reconstruction of the left and right MdLF (entire bundle) on a healthy subject (HCP_MGH_1017) based on the FA color-coding system (left and right panel) and projection of the reconstructed tracts on anatomical 3D T1 (middle panel): axial (upper left), coronal

(upper right) and sagittal (bottom) plane. Blue color at the edges of the fibers correspond to lower FA values as the fibers terminate on the cortical GM where FA is usually < 0.15 (Seehaus et al. 2015). L left, R right, MdLF middle longitudinal fasciculus

parts of the parallel “what” and “where” pathways, could reciprocally convey information to assist in the perception of sounds, possibly through changes in attentional biases. From a hodotopical standpoint, their common termination

areas in the TAr (Ding et al. 2009) and the supero-posterior parietal cortex could possibly function as hubs for the relay of information through a feed-forward and feed-back interaction. The MdLF-III in turn, which was found to connect

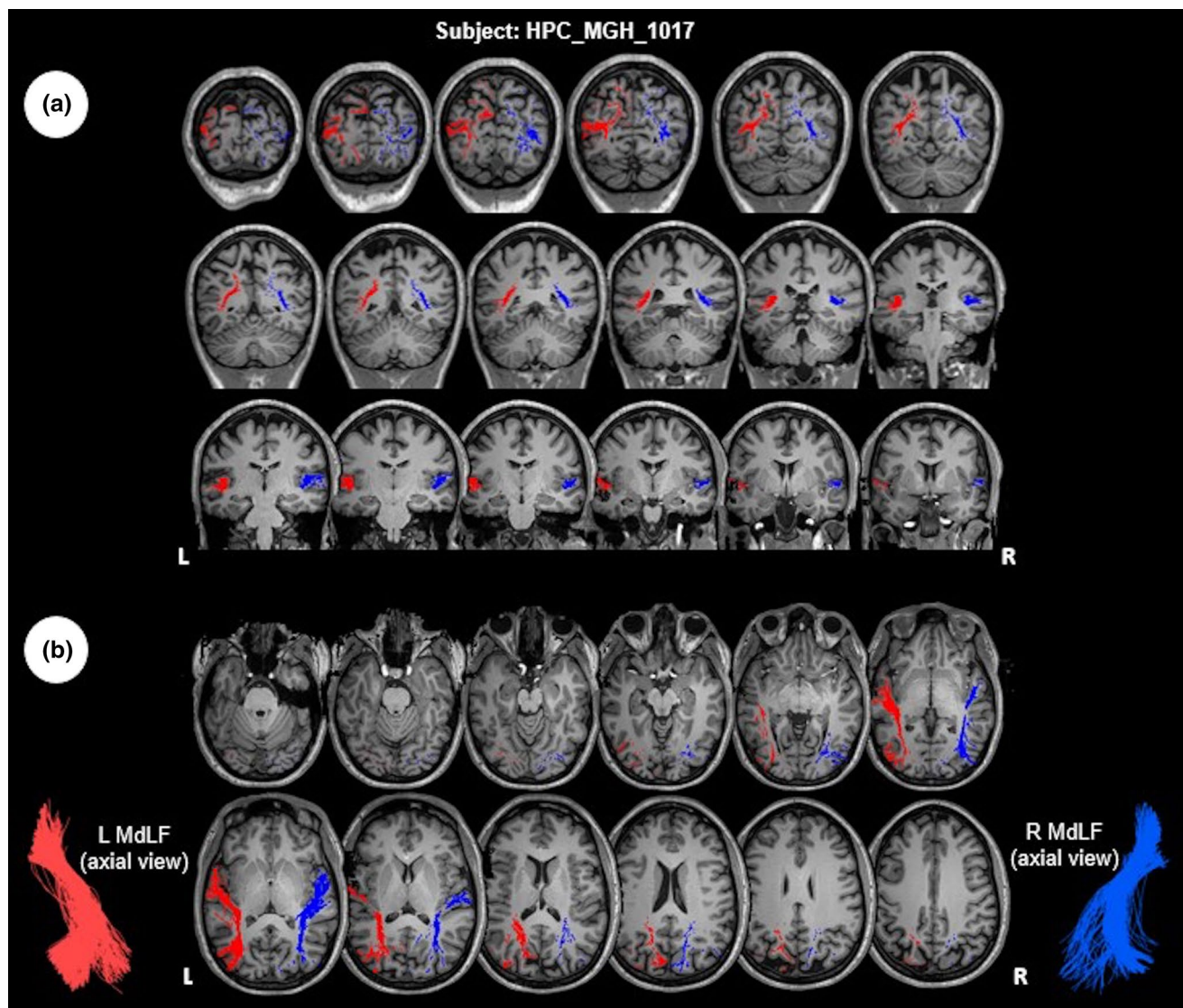


Fig. 10 Reconstruction of the left and right MdLF (entire bundle) and projection over subject's anatomical 3D T1 image on coronal (a) and axial (b) plane. Color-coding for the left (red) and right (blue) MdLF

is conventional for visualization purposes. *LL* left, *R* right, *MdLF* middle longitudinal fasciculus

the Polysensory area named as TAp (Ding et al. 2009; Seltzer and Pandya 1978, 1991) to the AG and occipital lobe/cuneus, could potentially play a role in the integration of auditory and visual information (Makris et al. 2017).

Finally, studies in patients with Semantic Dementia (Davies et al. 2004; Galton et al. 2001; Lambon Ralph and Patterson 2008; Mummery et al. 2000; Nestor et al. 2006; Noppeney et al. 2007) and herpes simplex virus encephalitis (HSVE) (Kapur et al. 1994; Lambon Ralph et al. 2007; Noppeney et al. 2007) as well as data from positron emission tomography (PET) (Devlin et al. 2000; Visser et al. 2010) and repetitive transcranial magnetic stimulation (rTMS) (Lambon Ralph et al. 2008; Pobric et al. 2007) in normal

participants point towards a potential role of the TP and anterior temporal lobe in semantic processing and auditory comprehension. More specifically, findings stemming from functional imaging implicate the anterior STG, near the anterior-lateral aspect of Heschl's gyrus, in sublexical processing and auditory word-form recognition (DeWitt and Rauschecker 2013, 2016). In the same vein, intraoperative brain mapping in 90 patients suggests that stimulation of the left STG leads to impairment of auditory single-word comprehension (Roux et al. 2015). Keeping with the putative role of MdLF in auditory processing and the fact that it represents an important subcortical connection of the STG, we could further postulate that it might serve as an

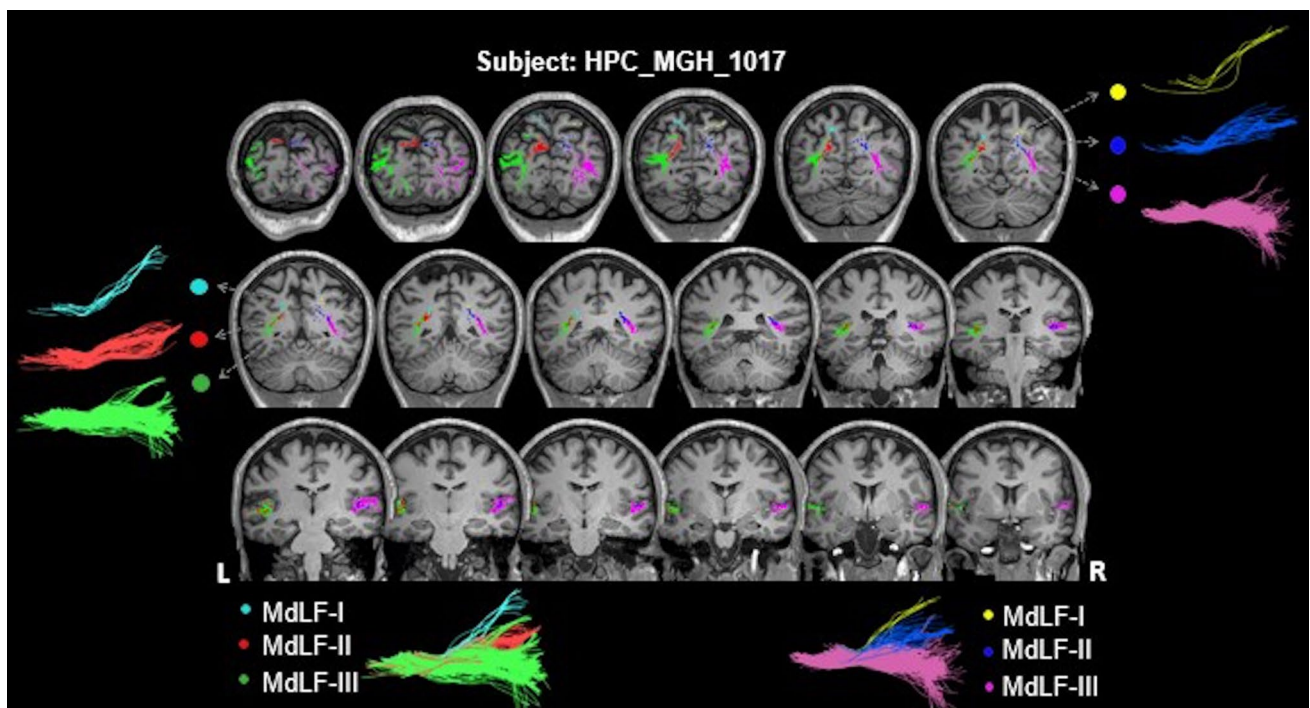


Fig. 11 Reconstruction of MdLF segments and projection over subject's anatomical 3D T1 (coronal plane). Color-coding for the left and the right MdLF segments is conventional for visualization purposes. *L* left, *R* right, *MdLF* middle longitudinal fasciculus

Fig. 12 Reconstruction of MdLF segments and projection over subject's anatomical 3D T1 (axial plane). Color-coding for the left and the right MdLF segments is conventional for visualization purposes. *L* left, *R* right, *MdLF* middle longitudinal fasciculus

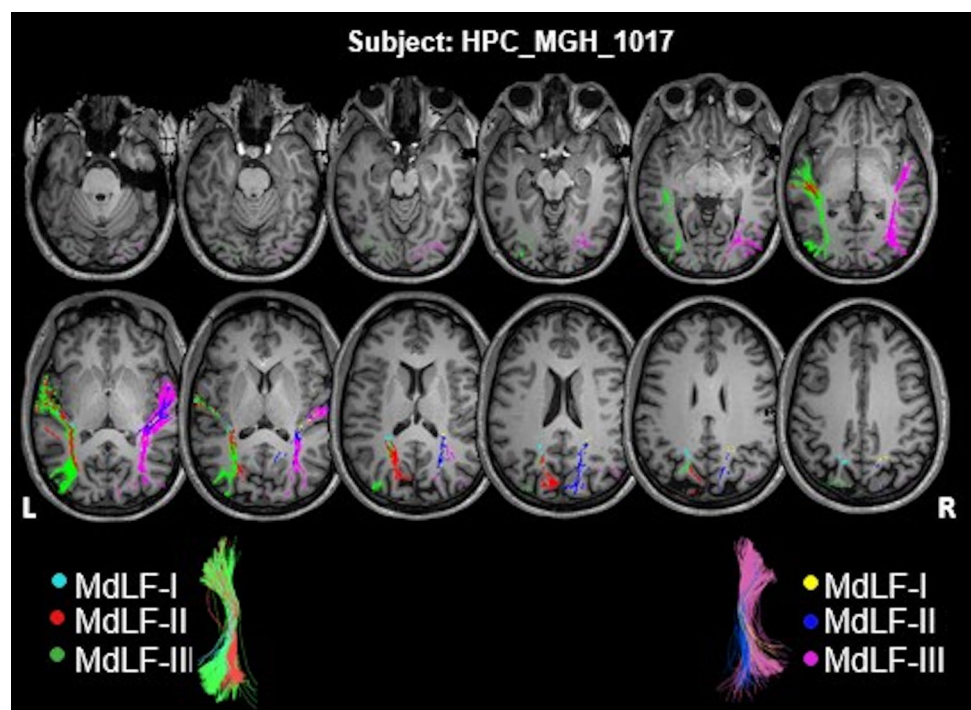


Fig. 13 Reconstruction of MdLF segments and projection over subject's anatomical 3D T1 (sagittal plane) for the left (a) and right (b) hemisphere. Color-coding for the left and the right MdLF segments is conventional for visualization purposes. *L* left, *R* right, *MdLF* middle longitudinal fasciculus

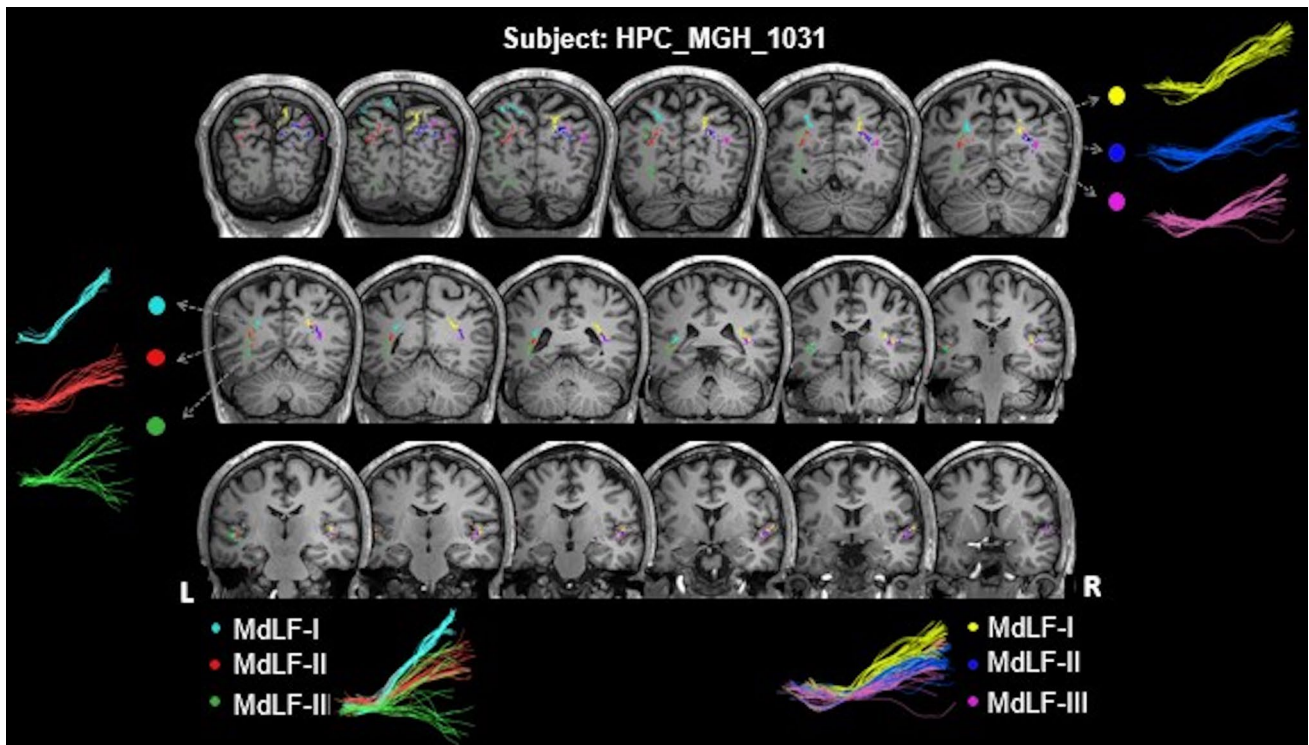
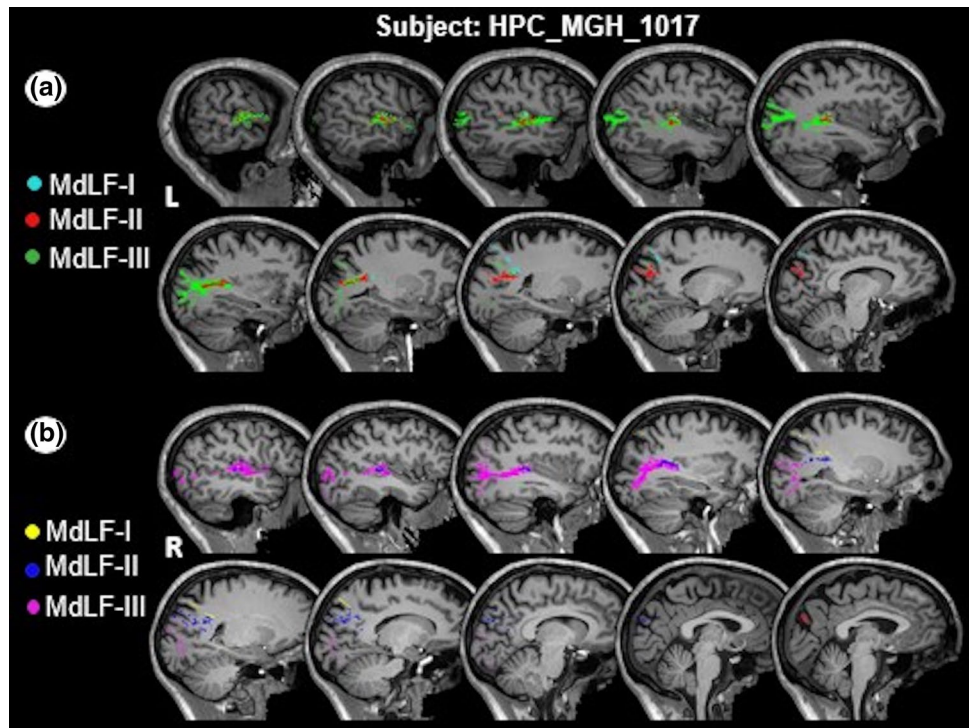


Fig. 14 Discrepancy of the pattern of posterior termination fibers. Reconstruction of MdLF segments and projection over subject's anatomical 3D T1 (coronal plane). Color-coding for the left and the right

MdLF segments is conventional for visualization purposes. *L* left, *R* right, *MdLF* middle longitudinal fasciculus

Table 1 Symmetry Index for mean FA, AD and RD for each subject for the entire MdLF and its segments

Subjects	SI											
	MdLF (entire)			MdLF-I			MdLF-II			MdLF-III		
	FA	AD	RD	FA	AD	RD	FA	AD	RD	FA	AD	RD
#1001	0.116	-0.004	-0.120	-0.092	-0.120	-0.056	0.085	-0.026	-0.109	0.182	0.041	-0.140
#1002	-0.011	-0.075	-0.061	0.066	0.024	-0.031	0.035	-0.024	-0.063	-0.006	-0.078	-0.071
#1003	-0.032	0.069	0.078	-0.037	0.058	0.088	0.070	0.177	0.116	-0.023	0.084	0.077
#1004	0.072	0.057	-0.047	0.030	0.004	0.048	0.007	0.004	0.014	0.074	0.052	-0.059
#1005	0.049	0.057	0.012	0.066	0.067	-0.006	0.092	0.171	0.047	0.086	0.075	0.002
#1006	0.008	-0.020	-0.019	0.024	0.023	-0.004	-0.039	-0.058	-0.004	0.020	-0.003	-0.019
#1007	-0.067	0.016	0.067	-0.068	-0.028	0.022	-0.002	1.533	0.021	-0.074	0.018	0.078
#1008	0.071	-0.068	-0.134	0.028	-0.063	-0.087	0.088	-0.051	-0.134	0.089	-0.103	-0.184
#1009	0.079	-0.022	-0.108	-0.006	-0.028	-0.035	0.061	-0.014	-0.076	0.118	-0.002	-0.133
#1010	-0.047	-0.007	0.034	-0.114	-0.005	0.090	0.018	0.015	-0.021	-0.049	-0.015	0.031
#1011	0.053	-0.006	-0.071	0.003	-0.018	-0.026	0.038	0.007	-0.020	0.058	0.000	-0.073
#1012	-0.039	-0.008	0.038	-0.061	-0.004	0.056	-0.036	0.005	0.050	-0.031	-0.003	0.028
#1013	0.098	-0.025	-0.126	0.037	-0.055	-0.102	0.115	0.028	-0.088	0.103	-0.050	-0.152
#1014	0.039	-0.033	-0.085	0.049	-0.032	-0.093	0.017	-0.015	-0.050	0.046	-0.041	-0.097
#1015	0.010	-0.023	-0.030	0.014	-0.009	-0.030	0.029	0.013	-0.025	0.060	0.011	-0.060
#1016	-0.118	0.005	0.150	-0.002	0.088	0.089	-0.036	-0.026	0.018	-0.124	0.005	0.163
#1017	0.156	-0.044	-0.181	0.015	-0.114	-0.122	0.079	-0.071	-0.144	0.177	-0.025	-0.188
#1018	-0.058	-0.008	0.041	-0.106	-0.020	0.075	-0.045	0.003	0.036	-0.066	-0.014	0.043
#1019	-0.113	0.025	0.132	-0.096	0.008	0.091	-0.092	0.060	0.140	-0.113	0.035	0.143
#1020	-0.039	0.010	0.038	-0.039	0.009	0.037	-0.083	-0.012	0.079	-0.014	0.039	0.050
#1021	0.128	0.021	-0.099	0.015	0.044	0.026	0.116	0.065	-0.058	0.130	0.013	-0.106
#1022	0.082	0.045	-0.043	0.029	0.000	-0.030	0.108	0.059	-0.057	0.095	0.052	-0.050
#1023	-0.010	0.125	0.126	0.041	0.171	0.119	-0.016	0.143	0.154	-0.012	0.105	0.129
#1024	-0.085	-0.066	0.019	-0.059	-0.100	0.005	-0.127	-0.100	0.030	-0.083	-0.067	0.017
#1025	-0.014	-0.016	-0.007	-0.022	-0.005	0.004	0.007	-0.022	-0.020	0.033	-0.008	-0.041
#1026	-0.074	-0.031	0.014	-0.107	-0.006	0.075	0.009	0.070	0.031	-0.056	0.026	0.062
#1027	-0.077	-0.043	0.041	-0.048	-0.036	0.017	-0.110	-0.045	0.028	-0.073	0.018	0.101
#1028	-0.094	0.058	0.145	-0.105	0.049	0.147	-0.102	0.043	0.136	-0.094	0.061	0.152
#1029	-0.050	-0.043	0.024	0.000	-0.010	0.004	-0.024	-0.011	0.022	-0.039	-0.048	0.015
#1030	0.027	-0.020	-0.046	0.034	-0.031	-0.062	-0.010	-0.007	-0.006	0.005	-0.033	-0.035
#1031	-0.020	0.039	0.047	0.006	0.054	0.035	-0.061	0.023	0.061	-0.019	0.048	0.061
#1032	0.098	-0.018	-0.111	0.034	-0.036	-0.042	0.118	-0.054	-0.167	0.115	-0.006	-0.115
#1033	0.077	0.013	-0.057	0.043	0.011	-0.044	0.125	0.041	-0.070	0.077	0.011	-0.059
#1034	0.031	-0.071	-0.081	0.109	-0.004	-0.087	-0.051	-0.148	-0.056	0.029	-0.065	-0.076
#1035	0.047	0.056	-0.006	0.015	0.043	0.006	0.054	0.034	-0.028	0.066	0.070	-0.001
Mean	0.008	-0.002	-0.012	-0.010	-0.002	0.005	0.012	0.052	-0.006	0.020	0.006	-0.014

MdLF middle longitudinal fasciculus, *MdLF-I* middle longitudinal fasciculus-segment I, *MdLF-II* middle longitudinal fasciculus-segment II, *MdLF-III* middle longitudinal fasciculus-segment III, *FA* fractional anisotropy, *AD* axial diffusivity, *RD* radial diffusivity, *SI* symmetry index

SI was calculated based on the formula : $(L - R)/(0.5 \times (L + R))$

anatomo-functional interface between auditory representations and semantic/lexical access.

Analysis of quantitative DTI metrics and symmetry

The range of the FA values calculated from the entire MdLF and its segments is in accordance with previous studies in

subcortical white matter tracts (Pierpaoli and Basser 1996). These values are slightly higher than the previously reported (Makris and Pandya 2009; Makris et al. 2013a, 2017; Menjot de Champfleury et al. 2013). In addition to inter-subject variability, differences in the extracted FA, AD and RD metrics can be also attributed to different DTI algorithms as reported in other studies focused either on central nervous system

Table 2 Descriptive measures for DTI indices of bilateral MdLF entire bundle and MdLF parts I–III

MdLF reconstructions	FA			AD			RD		
	Mean \pm SD	Median	CV %	Mean \pm SD	Median	CV %	Mean \pm SD	Median	CV %
Left hemisphere									
MdLF (entire)	0.47 \pm 0.03	0.47	6.81	1.21 $\times 10^{-3}$ \pm 6.72 $\times 10^{-5}$	1.20 $\times 10^{-3}$	5.54	5.64 $\times 10^{-4}$ \pm 5.37 $\times 10^{-5}$	5.66 $\times 10^{-4}$	9.52
MdLF-I	0.45 \pm 0.03	0.45	5.83	1.16 $\times 10^{-3}$ \pm 9.41 $\times 10^{-5}$	1.17 $\times 10^{-3}$	8.08	5.64 $\times 10^{-4}$ \pm 5.13 $\times 10^{-5}$	5.58 $\times 10^{-4}$	9.10
MdLF-II	0.47 \pm 0.03	0.47	6.60	1.23 $\times 10^{-3}$ \pm 1.05 $\times 10^{-4}$	1.22 $\times 10^{-3}$	8.55	5.67 $\times 10^{-4}$ \pm 5.60 $\times 10^{-5}$	5.65 $\times 10^{-4}$	9.87
MdLF-III	0.47 \pm 0.03	0.47	7.28	1.23 $\times 10^{-3}$ \pm 6.47 $\times 10^{-5}$	1.23 $\times 10^{-3}$	5.25	5.64 $\times 10^{-4}$ \pm 5.64 $\times 10^{-5}$	5.66 $\times 10^{-4}$	9.99
Right hemisphere									
MdLF (entire)	0.46 \pm 0.02	0.46	5.29	1.21 $\times 10^{-3}$ \pm 5.03 $\times 10^{-5}$	1.23 $\times 10^{-3}$	4.14	5.70 $\times 10^{-4}$ \pm 3.85 $\times 10^{-5}$	5.69 $\times 10^{-4}$	6.75
MdLF-I	0.45 \pm 0.02	0.45	4.46	1.16 $\times 10^{-3}$ \pm 6.20 $\times 10^{-5}$	1.16 $\times 10^{-3}$	5.32	5.60 $\times 10^{-4}$ \pm 3.49 $\times 10^{-5}$	5.59 $\times 10^{-4}$	6.23
MdLF-II	0.46 \pm 0.03	0.46	5.46	1.18 $\times 10^{-3}$ \pm 1.88 $\times 10^{-4}$	1.23 $\times 10^{-3}$	15.8	5.70 $\times 10^{-4}$ \pm 3.73 $\times 10^{-5}$	5.71 $\times 10^{-4}$	6.55
MdLF-III	0.46 \pm 0.03	0.46	5.81	1.23 $\times 10^{-3}$ \pm 5.65 $\times 10^{-5}$	1.23 $\times 10^{-3}$	4.6	5.71 $\times 10^{-4}$ \pm 3.98 $\times 10^{-5}$	5.68 $\times 10^{-4}$	6.97

MdLF middle longitudinal fasciculus, *MdLF-I* middle longitudinal fasciculus-segment I, *MdLF-II* middle longitudinal fasciculus-segment II, *MdLF-III* middle longitudinal fasciculus-segment III, *FA* fractional anisotropy, *AD* axial diffusivity, *RD* radial diffusivity, *SD* standard deviation, *CV* coefficient of variation

(Christidi et al. 2016; Feigl et al. 2014) or peripheral nervous system (Guggenberger et al. 2012) fiber tracts. Slightly elevated CV% of DTI metrics might indicate system (e.g., B0 inhomogeneity or gradient non-linearity) or radiographer (e.g., subject positioning, slice tilt)-related factors and/or increased inter-subject anatomical variability. However, increased variability in DTI indices using ROIs measures in different brain anatomical structures has also been reported in a well-designed study even when system—and user-related—errors were minimized (Veenith et al. 2013), which corroborates previous studies (Bisdas et al. 2008; Danielian et al. 2010; Heiervang et al. 2006; Takao et al. 2012). When SI was considered, we observed a rightward lateralization for the extracted DTI metrics in accordance with Menjot de Champfleury et al. (2013) but in contrast to the series of studies by Makris et al. (2009, 2013a, 2017). However, groupwise statistical analysis did not confirm any laterality differences as previously reported (Makris et al. 2009, 2013a; Makris et al. 2017). The profound functional role of both left and right MdLF might further explain the absence of significant differences.

Strengths and limitations of the study

Concerning the in vivo reconstruction of the entire MdLF and its segments, we applied a multi-ROI protocol in publicly available data from the HCP, which is fully described for replication and yielded high intra- and inter-rater reliability for the examined DTI indices. We additionally used a robust DTI algorithm, which has been previously shown to be reliable for the reconstruction of major associative, projection and commissural white matter tracts (Christidi et al. 2016), WM bundles arising from mediodorsal thalamic nuclei (Garibotto et al. 2019), relatively tiny hippocampal perforant pathway (Christidi et al. 2017), of and other

bundles that cannot be depicted with previous deterministic algorithms, such as the lateral cortical projections and crossing pontine fibers of the corticospinal tract (Christidi et al. 2016) and the crossing cortico-cerebellar tracts (Karavasilis et al. 2019). In a previous comparative dissection/DTI study, we have also observed that the placement of a single ROI on a highly contaminated region (such as the one between the superior frontal sulcus and the anterior-lateral ventricle) is able to reliably reconstruct fibers with different orientation (i.e., U-fibers; callosal fibers; external capsule; corticopontine fibers; thalamocortical fibers) (Koutsarnakis et al. 2017d). The reliability of reconstructed crossing, kissing and bending fibers has also been confirmed in a previous comparative study where the robustness of the algorithm was evaluated against a phantom DTI data; similar findings were observed between the ground truth and software reconstructed fibers (Karavasilis et al. 2019). Thus, despite the fact that crossing fibers are a major source of difficulty in DTI tractography, severe contaminations are hardly to affect our current findings.

DTI relies on the diffusion properties of water molecules along the direction of nerve axons and represents the only in vivo, fast, non-invasive but indirect method to map the cerebral white matter architecture. However, tractographic data may significantly vary due to several differences implicated in acquisition and post processing parameters (Jones and Cercignani 2010; Mori and Zhang 2006; Nimsy et al. 2016; Thomas et al. 2014). Additionally, this approach is prone to inaccurate results and artifacts since the reconstruction of erroneous white matter bundles cannot be fully prevented, particularly when tractography is applied to narrow and anatomically complex cerebral areas (Fernandez-Miranda et al. 2012; Johansen-Berg and Rushworth 2009; Le Bihan et al. 2006; Oouchi et al. 2007; Vos et al. 2011). Thus,

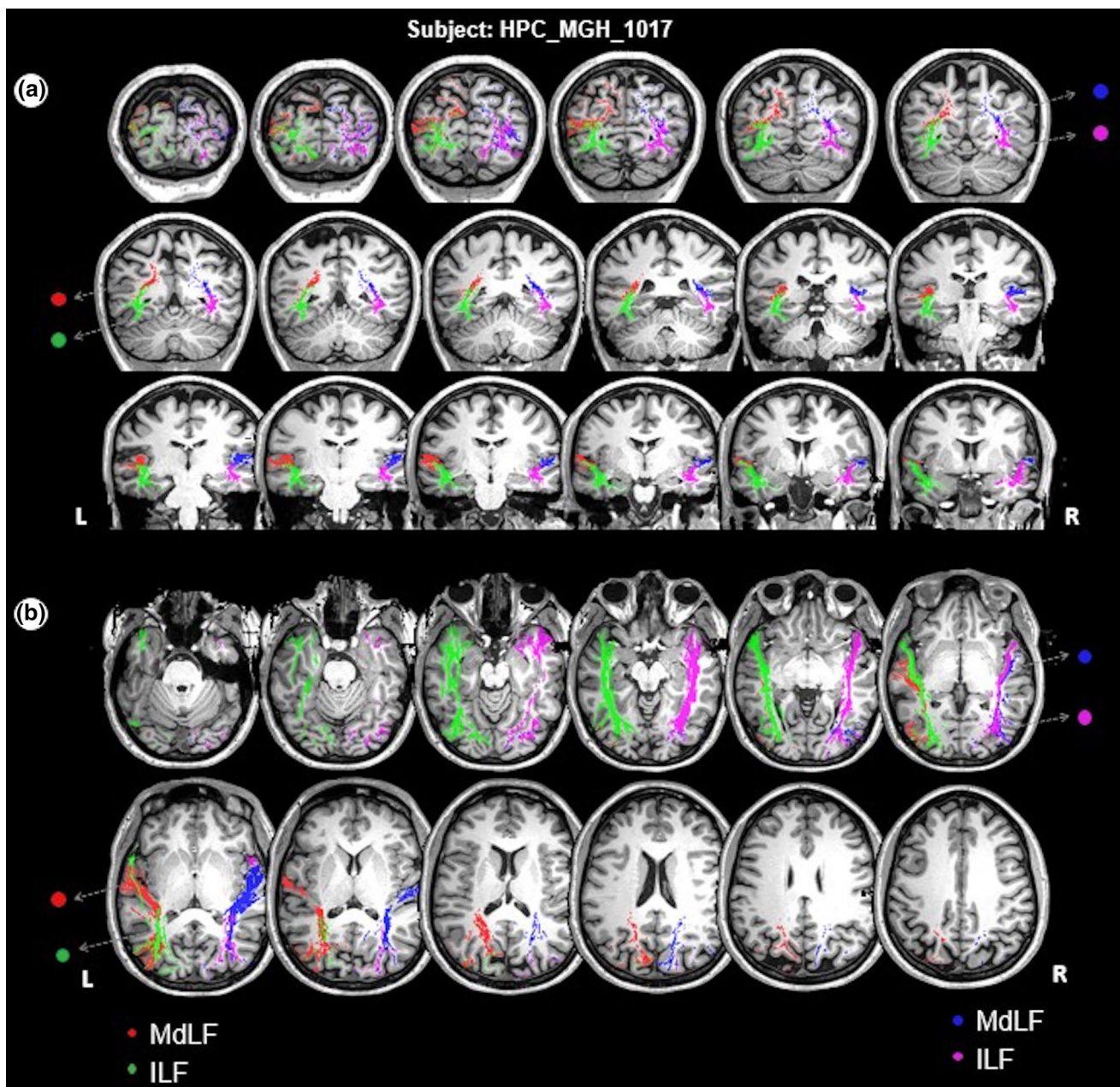


Fig. 15 Reconstruction of bilateral MdLF (entire bundle) and ILF and projection over subject's anatomical 3D T1 image on coronal (a) and axial (b) plane. Color-coding for the right and left MdLF (red and

blue, respectively) and right and left ILF (green and violet) is conventional for visualization purposes. *L* left, *R* right, *MdLF* middle longitudinal fasciculus, *ILF* inferior longitudinal fasciculus

DTI findings regarding under-studied fiber tracts have to be fully validated through other more robust methods.

The fiber dissection technique in turn, originally described by the Swiss anatomist Joseph Klingler, has

been recently incorporated into the field of neurocognitive research as a valuable tool offering new insights on the white matter and subcortical architecture (Klingler 1935). According to this resurgent method, the blunt cadaveric

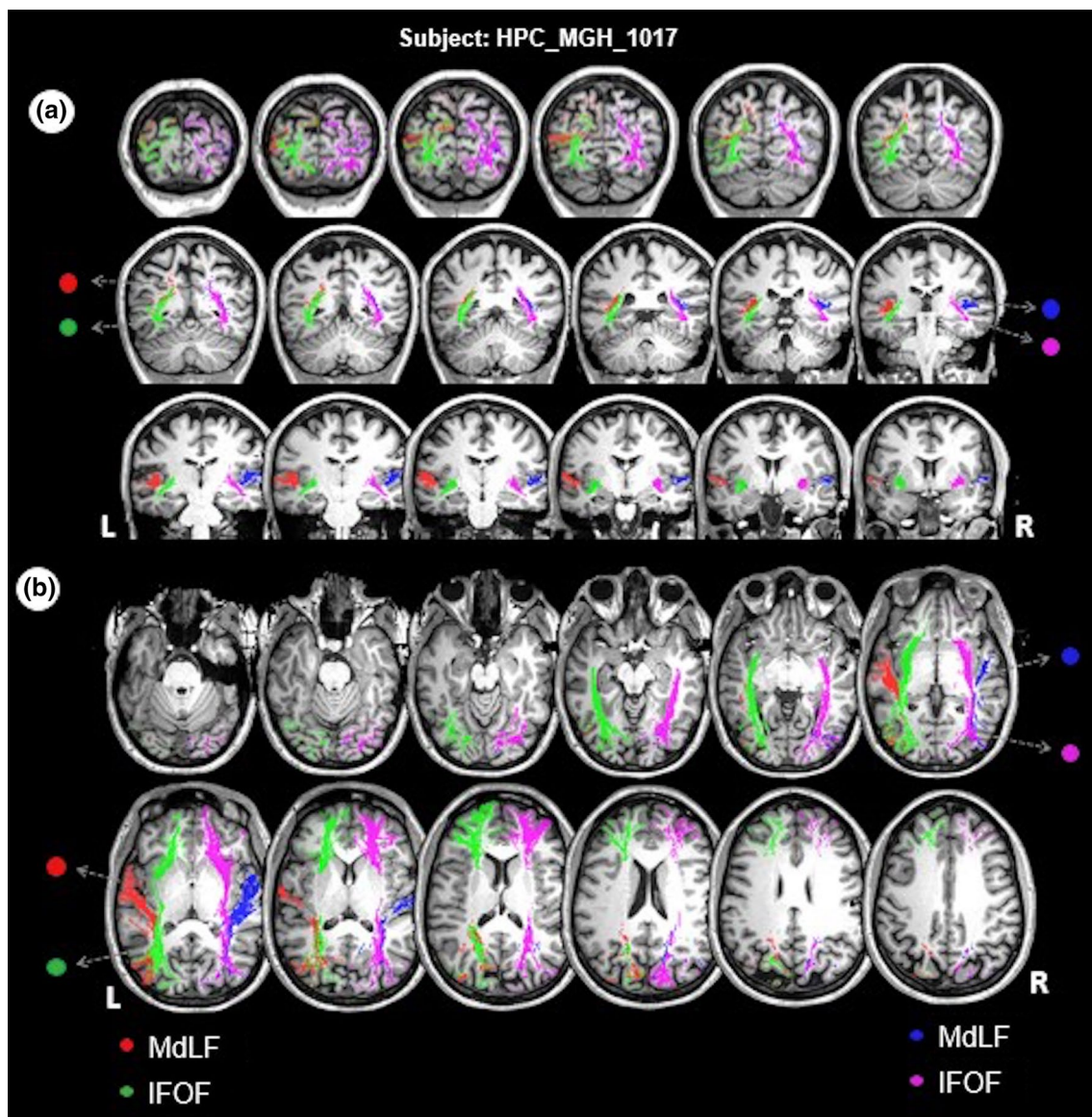


Fig. 16 Reconstruction of bilateral MdLF (entire bundle) and IFOF and projection over subject's anatomical 3D T1 image on coronal (a) and axial (b) plane. Color-coding for the right and left MdLF (red

and blue, respectively) and right and left IFOF (green and violet) is conventional for visualization purposes. *L* left, *R* right, *MdLF* middle longitudinal fasciculus, *IFOF* inferior fronto-occipital fasciculus

dissection of the white matter tracts is facilitated by the so-called “freeze–thaw preparation” since the ice crystals that form during the freezing process separate the white matter fibers apart (Klingler and Ludwig 1956). This freezing–defrosting process has been recently documented to preserve the structural integrity of white matter axons, interferes only with the extracellular matrix and therefore, the results obtained through this technique are considered highly reliable and accurate (Zemmoura et al. 2016). In addition, the development of the so-called “cortex sparing technique”, which is actually a modification of the basic Klingler method, further allows the proper investigation of the termination and connectivity pattern of the subcortical

fiber pathways (Martino et al. 2011). As such, the fiber dissection technique is currently considered as the gold standard method for validating data stemming from DTI studies and has, thus, been extensively used by the authors of this study for exploring and mapping the fiber tract architecture (Komaitis et al. 2019; Koutsarnakis et al. 2015, 2017a, b, c, d, 2018, 2019; Liakos and Koutsarnakis 2016). Although several sophisticated algorithms and high-resolution DWI data are currently available mostly for research use, ex vivo approaches including axonal tracing and dissection remain the most reliable method to unveil distinct WM bundles. The Klingler’s dissection is deemed as the only available technique to directly study the WM fibers at macroscopic

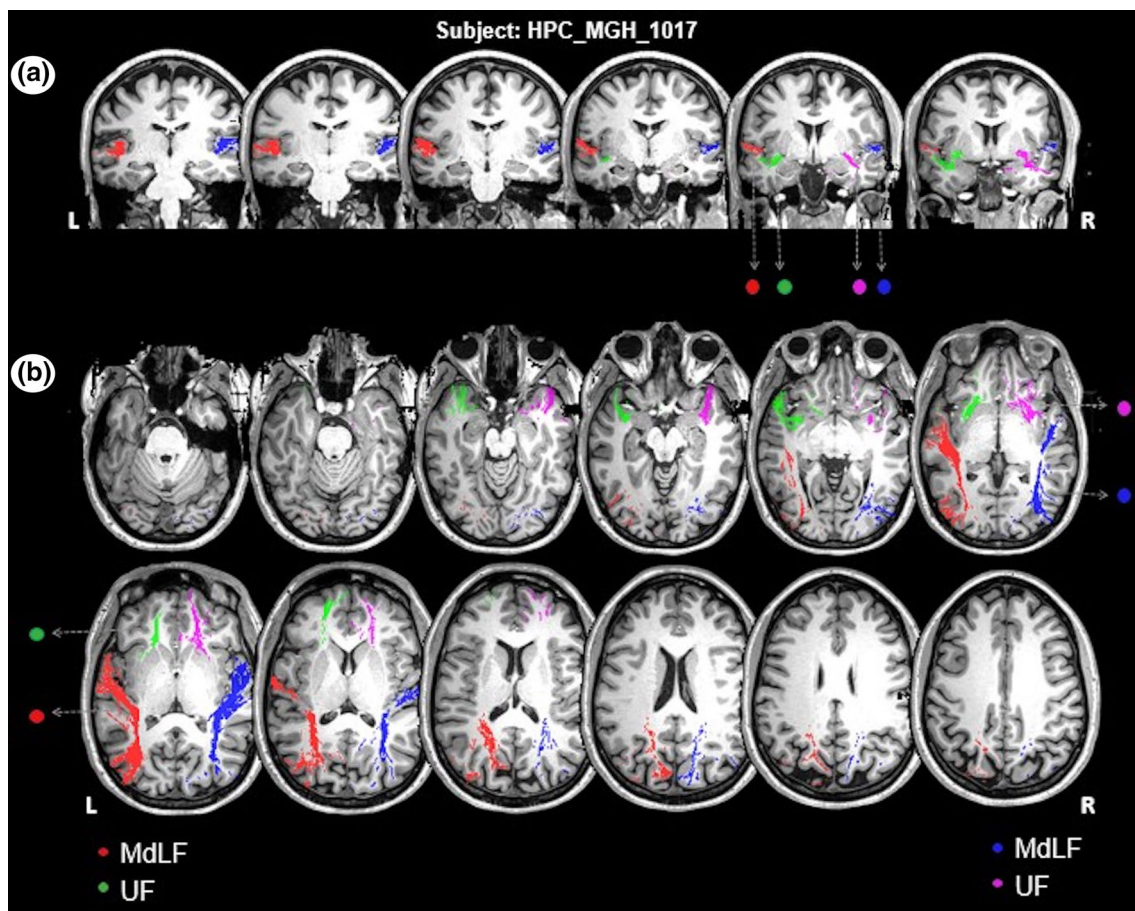


Fig. 17 Reconstruction of bilateral MdLF (entire bundle) and UF and projection over subject's anatomical 3D T1 image on coronal (a) and axial (b) plane. Color-coding for the right and left MdLF (red and

blue, respectively) and right and left UF (green and violet) is conventional for visualization purposes. *L* left, *R* right, *MdLF* middle longitudinal fasciculus, *UF* uncinate fasciculus

level (Mandonnet et al. 2018) and continues to be used in several dissection or DTI/dissection papers that study a wide range of white matter tracts (Altieri et al. 2019; De Benedictis et al. 2014; Di Carlo et al. 2019; Flores-Justa et al. 2019; Holl et al. 2011; Nachtergaele et al. 2019; Pescatori et al. 2017; Shah et al. 2019; Wu et al. 2016). Combined methodological approaches that integrate ex vivo methods and DTI tractography with high-quality data are definitely warranted to produce the most accurate map of the brain connectome (Thomas et al. 2014).

However, apart from being an in vitro, expensive and very delicate procedure, this method provides lower spatial resolutions when compared to histology and optical coherence tomography (Palm et al. 2010; Wang et al. 2011). Further and most importantly, the method's accuracy may decrease when studying the structural relationship of crossing fiber tracts, since the proper dissection of one usually interferes with the anatomical integrity of the other.

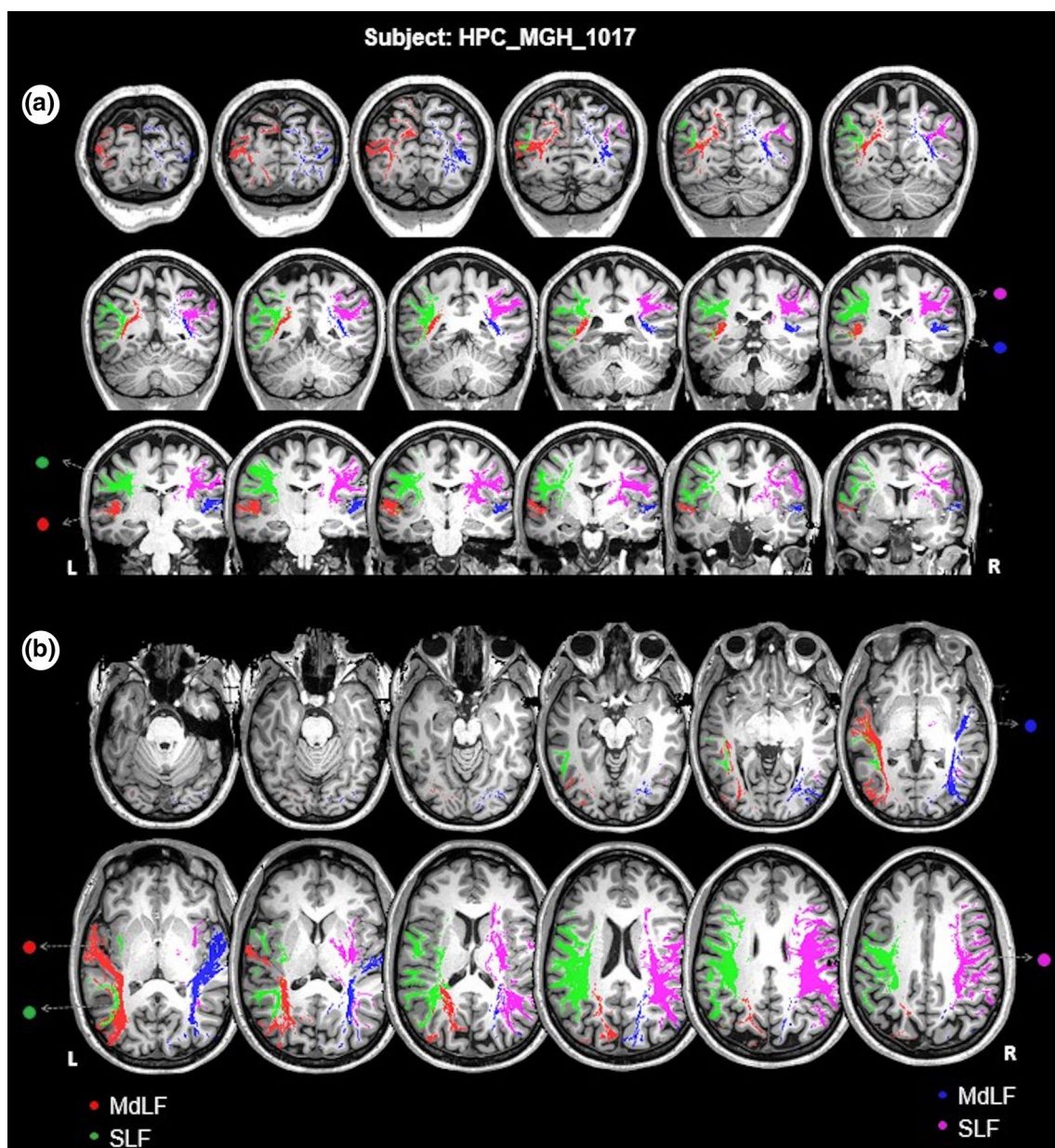


Fig. 18 Reconstruction of bilateral MdLF (entire bundle) and SLF and projection over subject's anatomical 3D T1 image on coronal (a) and axial (b) plane. Color-coding for the right and left MdLF (red

and blue, respectively) and right and left SLF (green and violet) is conventional for visualization purposes. *L* left, *R* right, *MdLF* middle longitudinal fasciculus, *SLF* superior longitudinal fasciculus

Conclusions

Focused fiber micro-dissections augmented by a tailored DTI protocol on the publicly available dataset from the Human Connectome Project were employed to clarify the structural architecture of a recently identified tract known

as the MdLF. The applied multi-ROI protocol yielded high intra- and inter-rater reliability for the examined DTI indices, while the dissection and tractographic findings showed a good correspondence regarding the MdLF topography, morphology and axonal connectivity. Our results draw on the robust anterior terminations of MdLF to specific subregions

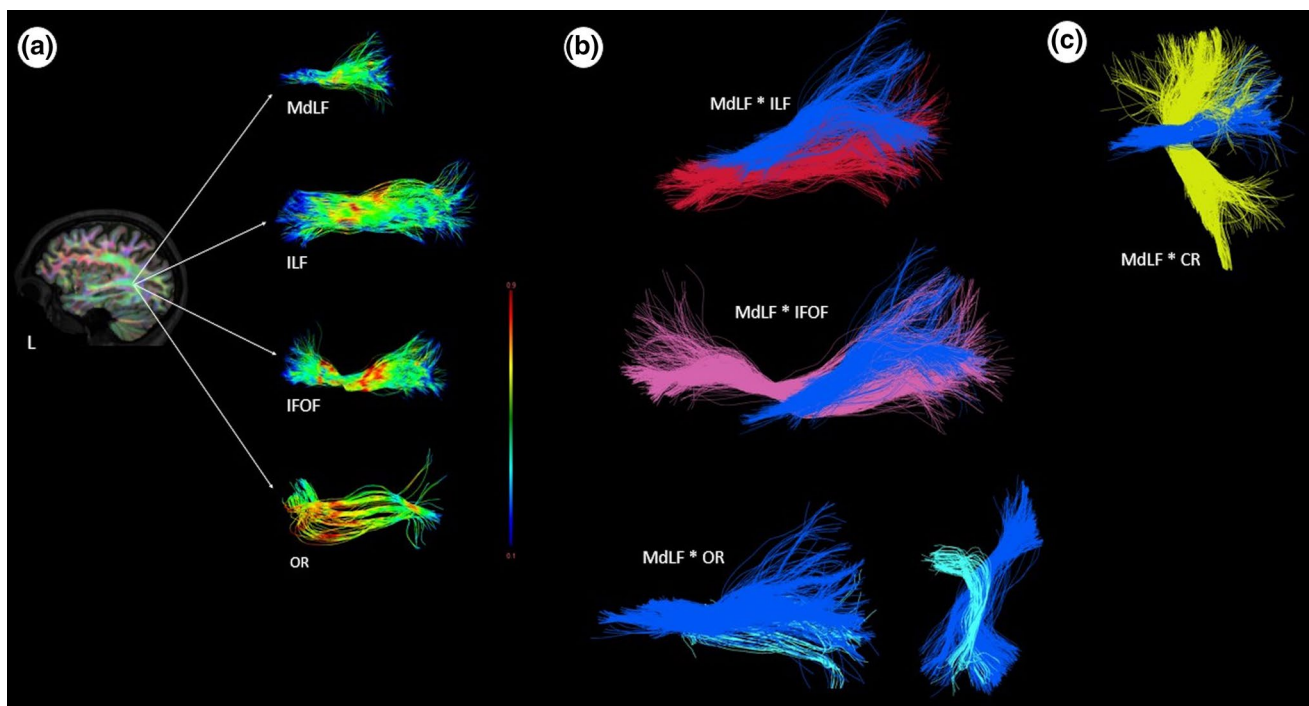


Fig. 19 **a** WM tracts that pass through different layers of sagittal stratum (Di Carlo et al. 2019): MdLF and ILF (superficial layer); IFOF (middle layer); OR (deep layer). (WM tracts are depicted using the FA color-coding system. Blue colour at the edges of each tract corresponds to low FA due to the termination areas of the bundles on cortical GM). **b** Areas of intersection between MdLF and ILF (upper panel; sagittal view), MdLF and IFOF (middle panel; sagittal view) and MdLF and OR (lower panel; sagittal and axial view) in left-reconstructed tracts. **c** Areas of intersection between MdLF and CR in left-reconstructed tracts. Color-coding system in **(b, c)** is conventional for visualization purposes. *WM* white matter, *MdLF* middle longitudinal fasciculus, *ILF* inferior longitudinal fasciculus, *IFOF* inferior longitudinal fasciculus, *OR* optic radiation, *CR* coronal radiata, *L* left, *FA* fractional anisotropy

tal view) and MdLF and OR (lower panel; sagittal and axial view) in left-reconstructed tracts. **c** Areas of intersection between MdLF and CR in left-reconstructed tracts. Color-coding system in **(b, c)** is conventional for visualization purposes. *WM* white matter, *MdLF* middle longitudinal fasciculus, *ILF* inferior longitudinal fasciculus, *IFOF* inferior longitudinal fasciculus, *OR* optic radiation, *CR* coronal radiata, *L* left, *FA* fractional anisotropy

of the TP, the intrinsic anatomical relationship of the tract to the auditory cortex and the lack of significant connections with the IPL (SMG and AG). The lack of leftward asymmetry and rich connectivity with the IPL along with data from direct intraoperative stimulation tend to shift the paradigm away from language function. Conversely, in light of the theory of parallel “where” and “what” auditory pathways, the strong relationship of the MdLF with the auditory cortex

and the functional role of the cortical areas that it interconnects tend to shift the paradigm towards auditory function. Allegedly, the MdLF-I and MdLF-II as parts of the parallel “what” and “where” pathways, respectively, may play a role in the perception of sounds; whereas, the MdLF-III could underpin the integration of auditory and visual information. Since recent data support the notion that the TP and anterior STG should be treated as “hubs” for semantic

Table 3 Middle Longitudinal Fasciculus connectivity, segmentation, and putative function according to the published studies focusing on MdLF

Authors (year)/Journal	Methods of identification/subjects (males) [Mean age or range]	Connectivity	Segmentation	Potential function
Makris et al. (2009)/Cerebral Cortex	DTI/4 (2) [23–33]	TP, STG, AG	1 segment	Language and attention
Makris et al. (2013a)/Brain structure and function	DTI/39 (35) [34.8]	TP, STG, SMG, AG, SPL, PrC, TPOC, OL	1 segment (many patterns)	Language, Visuospatial attention, high-order auditory and visual function
Makris et al. (2013b)/Brain imaging and behavior	DTI/74 (62) [24.9]	TP, STG, AG, SPL	2 Segments STG-AG STG-SPL	Language (STG-AG), attention (STG-AG), visuospatial and integrative audiovisual functions (STG-SPL)
Maldonado et al. (2013)/Journal of Anatomy	WMD/18 Hemispheres 9 Right and 9 Left	STG, OL	1 segment	MdLF may participate but is not believed to be essential for language processing
Menjot de Champfleure et al. (2013)/European Journal of Radiology	DTI/4 (2) [28.5]	TP, STG, AG, OL	1 segment	The MdLF is not regarded as a main pathway in language processing but rather is believed to participate in a parallel transmodal neuro-cognitive network.
Wang et al. (2013)/Cerebral Cortex	WMD/8 Hemispheres (1) [32–81] and DTI/6 (5) [22–31]	TP, STG, SPL, PrC, OL, C, Minor connections to AG	2 Segments: STG-SPL/PrC STG-OCL/C (deep)	Rather than a language-related tract, the MdLF may contribute to the dorsal pathway of the auditory system
Makris et al. (2017)/Brain imaging and behavior	DTI/70 (59) [34]	TP, STG, SMG, AG, SPL, PrC, OL, C	6 Segments STG-AG STG-SMG STG-SPL STG-PrC STG-C STG-LOCL	Language, attention, high-order auditory and integrative audiovisual functions STG-AG: Language and attention. Mapping sub-lexical representations onto articulatory forms. Also acoustic-phonetic processing of words and word production. STG-SMG: Language and attention. Phonetic processing
Conner et al. (2018)/Operative Neurosurgery	DTI/10 (-) [-]	STG, STS, SPL, IPS, C, Li	1 segment	Auditory processing, auditory organization, and possibly visuospatial function and working memory. May have a role in language function
Tremblay et al. (2019)/Human Brain Mapping	DTI/29 (21) [19–84]	TP, STG, IPL, SPL	2 segments: TP/STG-IPL TP/STG-SPL.	The MdLF is important for speech perception in noise The right MdLF- SPL is related to response bias

AG angular gyrus, C cuneus, DTI diffusion tensor imaging, IPL inferior parietal lobule, IPS inferior parietal sulcus, Li lingual gyrus, MdLF middle longitudinal fasciculus, OL occipital lobe, PrC precuneus, SMG supramarginal gyrus, SPL superior parietal lobule, STG superior temporal gyrus, TP temporal pole, TPOC temporo-parieto-occipital area

processing and auditory word-form recognition, the working hypothesis viewing the MdLF as an anatomic-functional interface between auditory representations and semantic/lexical access gains further ground.

Author contributions Author contributions to the study and manuscript preparation include the following. Conception and design: Kalyvas, Koutsarnakis. Acquisition of data: Kalyvas, Koutsarnakis, Komaitis, Karavasilis, Christidi, Papakostantinou, Kelekis. Analysis and interpretation of data: Kalyvas, Koutsarnakis, Christidi, Karavasilis, Komaitis, Liouta, Skandalakis. Drafting the article: Koutsarnakis, Kalyvas, Christidi, Karavasilis. Critically revising the article: Koutsarnakis, Kalyvas, Duffau, Stranjalis. Reviewed submitted version of manuscript: All authors. Administrative technical, material support: Koutsarnakis, Stranjalis. Study supervision: Koutsarnakis.

Funding No funding was received for this study.

Compliance with ethical standards

Conflict of interest The authors declare that they have no conflict of interest.

References

- Ahveninen J et al (2006) Task-modulated “what” and “where” pathways in human auditory cortex. *Proc Natl Acad Sci U S A* 103:14608–14613. <https://doi.org/10.1073/pnas.0510480103>
- Altieri R et al (2019) Inferior fronto-occipital fascicle anatomy in brain tumor surgeries: from anatomy lab to surgical theater. *J Clin Neurosci* 68:290–294. <https://doi.org/10.1016/j.jocn.2019.07.039>
- Alves RV, Ribas GC, Parraga RG, de Oliveira E (2012) The occipital lobe convexity sulci and gyri. *J Neurosurg* 116:1014–1023. <https://doi.org/10.3171/2012.1.JNS11978>
- Basser PJ, Mattiello J, LeBihan D (1994) MR diffusion tensor spectroscopy and imaging. *Biophys J* 66:259–267
- Binder JR, Frost JA, Hammeke TA, Bellgowan PS, Springer JA, Kaufman JN, Possing ET (2000) Human temporal lobe activation by speech and nonspeech sounds. *Cereb cortex* 10:512–528
- Bisdas S, Bohning DE, Besenski N, Nicholas JS, Rumboldt Z (2008) Reproducibility, interrater agreement, and age-related changes of fractional anisotropy measures at 3T in healthy subjects: effect of the applied b-value. *AJNR Am J Neuroradiol* 29:1128–1133. <https://doi.org/10.3174/ajnr.a1044>
- Brunetti M et al (2005) Human brain activation during passive listening to sounds from different locations: an fMRI and MEG study. *Hum Brain Mapp* 26:251–261
- Bullock D, Takemura H, Caiafa CF, Kitchell L, McPherson B, Caron B, Pestilli F (2019) Associative white matter connecting the dorsal and ventral posterior human cortex. *Brain Struct Funct* 224:2631–2660. <https://doi.org/10.1007/s00429-019-01907-8>
- Burks JD et al (2017) White matter connections of the inferior parietal lobule: A study of surgical anatomy. *Brain Behav* 7:e00640. <https://doi.org/10.1002/brb3.640>
- Catani M, Catani M (2007) From hodology to function. *Brain* 130:602–605
- Catani M, De Schotten MT (2008) A diffusion tensor imaging tractography atlas for virtual in vivo dissections. *Cortex* 44:1105–1132
- Catani M, Howard RJ, Pajevic S, Jones DK (2002) Virtual in vivo interactive dissection of white matter fasciculi in the human brain. *Neuroimage* 17:77–94
- Catani M, Allin MP, Husain M, Pugliese L, Mesulam MM, Murray RM, Jones DK (2007) Symmetries in human brain language pathways correlate with verbal recall. *Proc Natl Acad Sci USA* 104:17163–17168. <https://doi.org/10.1073/pnas.0702116104>
- Christidi F, Karavasilis E, Samiotis K, Bisdas S, Papanikolaou N (2016) Fiber tracking: A qualitative and quantitative comparison between four different software tools on the reconstruction of major white matter tracts. *Eur J Radiol Open* 3:153–161. <https://doi.org/10.1016/j.ejro.2016.06.002>
- Christidi F et al (2017) Memory-related white matter tract integrity in amyotrophic lateral sclerosis: an advanced neuroimaging and neuropsychological study. *Neurobiol Aging* 49:69–78. <https://doi.org/10.1016/j.neurobiolaging.2016.09.014>
- Conner AK et al (2018) A connectomic atlas of the human cerebrum—chapter 12: tractographic description of the middle longitudinal fasciculus. *Oper Neurosurg (Hagerstown)* 15:S429–S435. <https://doi.org/10.1093/ons/opy266>
- Danielian LE, Iwata NK, Thomasson DM, Floeter MK (2010) Reliability of fiber tracking measurements in diffusion tensor imaging for longitudinal study. *Neuroimage* 49:1572–1580. <https://doi.org/10.1016/j.neuroimage.2009.08.062>
- Davies R, Graham KS, Xuereb JH, Williams GB, Hodges JR (2004) The human perirhinal cortex and semantic memory. *Eur J Neurosci* 20:2441–2446
- De Benedictis A, Duffau H (2011) Brain hodotopy: from esoteric concept to practical surgical applications. *Neurosurgery* 68:1703–1723
- De Benedictis A et al (2014) Anatomic-functional study of the temporoparieto-occipital region: dissection, tractographic and brain mapping evidence from a neurosurgical perspective. *J Anat* 225:132–151. <https://doi.org/10.1111/joa.12204>
- De Witt Hamer PC, Moritz-Gasser S, Gatignol P, Duffau H (2011) Is the human left middle longitudinal fascicle essential for language? A brain electrostimulation study. *Human brain mapping* 32:962–973
- Dejerine J, Dejerine-Klumpke A (1895) Anatomie des centres nerveux: Méthodes générales d’étude-embryologie-histogénèse et histologie. Anatomie du cerveau vol 1. Rueff,
- Devlin JT et al (2000) Susceptibility-induced loss of signal: comparing PET and fMRI on a semantic task. *Neuroimage* 11:589–600
- DeWitt I, Rauschecker JP (2013) Wernicke’s area revisited: parallel streams and word processing. *Brain Lang* 127:181–191
- DeWitt I, Rauschecker JP (2016) Convergent evidence for the causal involvement of anterior superior temporal gyrus in auditory single-word comprehension. *Cortex* 77:164–166
- Di Carlo DT et al (2019) Microsurgical anatomy of the sagittal stratum. *Acta Neurochir (Wien)*. <https://doi.org/10.1007/s00701-019-04019-8>
- Ding SL, Van Hoesen GW, Cassell MD, Poremba A (2009) Parcellation of human temporal polar cortex: a combined analysis of multiple cytoarchitectonic, chemoarchitectonic, and pathological markers. *J Comp Neurol* 514:595–623. <https://doi.org/10.1002/cne.22053>
- Duffau H (2011) Brain mapping: from neural basis of cognition to surgical applications. Springer Science & Business Media, Berlin
- Duffau H, Duffau H (2010) Awake surgery for non-language mapping Neurosurgery
- Feigl GC et al (2014) Magnetic resonance imaging diffusion tensor tractography: evaluation of anatomic accuracy of different fiber tracking software packages. *World Neurosurg* 81:144–150. <https://doi.org/10.1016/j.wneu.2013.01.004>

- Fernandez-Miranda JC et al (2012) High-definition fiber tractography of the human brain: neuroanatomical validation and neurosurgical applications. *Neurosurgery* 71:430–453. <https://doi.org/10.1227/NEU.0b013e3182592faa>
- Filley CM (1998) The behavioral neurology of cerebral white matter. *Neurology* 50:1535–1540
- Filley CM (2005) White matter and behavioral neurology. *Ann NY Acad Sci* 1064:162–183. <https://doi.org/10.1196/annals.1340.028>
- Flores-Justa A, Baldoncini M, Perez Cruz JC, Sanchez Gonzalez F, Martinez OA, Gonzalez-Lopez P, Campero A (2019) White matter topographic anatomy applied to temporal lobe surgery. *World Neurosurg*. <https://doi.org/10.1016/j.wneu.2019.08.050>
- Galati G, Committeri G, Sanes JN, Pizzamiglio L (2001) Spatial coding of visual and somatic sensory information in body-centred coordinates. *Eur J Neurosci* 14:737–746
- Galletti C, Fattori P (2002) Posterior parietal networks encoding visual space
- Galton CJ et al (2001) Differing patterns of temporal atrophy in Alzheimer's disease and semantic dementia. *Neurology* 57:216–225
- Garibotto V, Wissmeyer M, Giavri Z, Ratib O, Picard F (2019) Nicotinic acetylcholine receptor density in the “Higher-Order” thalamus projecting to the prefrontal cortex in humans: a PET Study. *Mol Imaging Biol*. <https://doi.org/10.1007/s11307-019-01377-8>
- Gow DW Jr, Segawa JA, Ahlfors SP, Lin F-H (2008) Lexical influences on speech perception: a Granger causality analysis of MEG and EEG source estimates. *Neuroimage* 43:614–623
- Guggenberger R, Nanz D, Puijpe G, Ruffbach K, White LM, Sussman MS, Andreisek G (2012) Diffusion tensor imaging of the median nerve: intra-, inter-reader agreement, and agreement between two software packages. *Skelet Radiol* 41:971–980. <https://doi.org/10.1007/s00256-011-1310-4>
- Gungor A, Baydin S, Middlebrooks EH, Tanriover N, Isler C, Rhoton AL Jr (2017) The white matter tracts of the cerebrum in ventricular surgery and hydrocephalus. *J Neurosurg* 126:945–971. <https://doi.org/10.3171/2016.1.JNS152082>
- Hackett TA, Stepniewska I, Kaas JH (1999) Prefrontal connections of the parabelt auditory cortex in macaque monkeys. *Brain Res* 817:45–58
- Heierwang E, Behrens TE, Mackay CE, Robson MD, Johansen-Berg H (2006) Between session reproducibility and between subject variability of diffusion MR and tractography measures. *Neuroimage* 33:867–877. <https://doi.org/10.1016/j.neuroimage.2006.07.037>
- Hickok G, Poeppel D (2007) The cortical organization of speech processing. *Nat Rev Neurosci* 8:393–402. <https://doi.org/10.1038/nrn2113>
- Holl N et al (2011) Temporal lobe association fiber tractography as compared to histology and dissection. *Surg Radiol Anat* 33:713–722. <https://doi.org/10.1007/s00276-011-0816-8>
- Howard MA 3rd, Volkov IO, Abbas PJ, Damasio H, Ollendieck MC, Granner MA (1996) A chronic microelectrode investigation of the tonotopic organization of human auditory cortex. *Brain Res* 724:260–264
- Howard MA et al (2000) Auditory cortex on the human posterior superior temporal gyrus. *J Comp Neurol* 416:79–92
- Zemmoura I, Blanchard E, Raynal P-I, Rousselot-Denis C, Destrieux C, Velut S (2016) How Klingler's dissection permits exploration of brain structural connectivity? An electron microscopy study of human white matter. *Brain Struct Funct* 221:2477–2486
- Jääskeläinen IP et al (2004) Human posterior auditory cortex gates novel sounds to consciousness. *Proc Natl Acad Sci* 101:6809–6814
- Johansen-Berg H, Rushworth MF (2009) Using diffusion imaging to study human connective anatomy. *Annu Rev Neurosci* 32:75–94. <https://doi.org/10.1146/annurev.neuro.051508.135735>
- Jones DK, Cercignani M (2010) Twenty-five pitfalls in the analysis of diffusion MRI data. *NMR Biomed* 23:803–820. <https://doi.org/10.1002/nbm.1543>
- Kamali A, Flanders AE, Brody J, Hunter JV, Hasan KM (2014) Tracing superior longitudinal fasciculus connectivity in the human brain using high resolution diffusion tensor tractography. *Brain Struct Funct* 219:269–281. <https://doi.org/10.1007/s00429-012-0498-y>
- Kapur N et al (1994) Herpes simplex encephalitis: long term magnetic resonance imaging and neuropsychological profile. *J Neurol Neurosurg Psychiatry* 57:1334–1342
- Karavasilis E et al (2019) Ipsilateral and contralateral cerebro-cerebellar white matter connections: a diffusion tensor imaging study in healthy adults. *J Neuroradiol* 46:52–60. <https://doi.org/10.1016/j.neurad.2018.07.004>
- Keil B et al (2013) A 64-channel 3T array coil for accelerated brain MRI. *Magn Reson Med* 70:248–258. <https://doi.org/10.1002/mrm.24427>
- Klingler J (1935) Erleichterung der makroskopischen Präparation des Gehirns durch den Gefrierprozess. Orell Füssli, Zurich
- Klingler J, Ludwig E (1956) Atlas cerebri humani. Karger Publishers, Basel
- Komaitis S et al (2019) Dorsal component of the superior longitudinal fasciculus revisited: novel insights from a focused fiber dissection study *J Neurosurg*. <https://doi.org/10.3171/2018.11.jns182908>
- Koutsarnakis C, Liakos F, Kalyvas AV, Sakas DE, Stranjalis G (2015) A laboratory manual for stepwise cerebral white matter fiber dissection. *World Neurosurg* 84:483–493. <https://doi.org/10.1016/j.wneu.2015.04.018>
- Koutsarnakis C, Kalyvas AV, Stranjalis G (2017a) Letter to the editor: approaches to the ventricular atrium. *J Neurosurg* 126:1373–1374
- Koutsarnakis C, Liakos F, Kalyvas AV, Komaitis S, Stranjalis G (2017b) Letter to the Editor: white matter fiber tract architecture and ventricular surgery. *J Neurosurg* 126:1368–1371
- Koutsarnakis C et al (2017c) Approaching the atrium through the intraparietal sulcus: mapping the sulcal morphology and correlating the surgical corridor to underlying fiber tracts. *Oper Neurosurg (Hagerstown)* 13:503–516. <https://doi.org/10.1093/ons/0pw037>
- Koutsarnakis C et al (2017d) The superior frontal transsulcal approach to the anterior ventricular system: exploring the sulcal and subcortical anatomy using anatomic dissections and diffusion tensor imaging tractography. *World Neurosurg* 106:339–354. <https://doi.org/10.1016/j.wneu.2017.06.161>
- Koutsarnakis C, Kalyvas AV, Komaitis S, Liakos F, Skandalakis GP, Anagnostopoulos C, Stranjalis G (2018) Defining the relationship of the optic radiation to the roof and floor of the ventricular atrium: a focused microanatomical study. *J Neurosurg*. <https://doi.org/10.3171/2017.10.jns171836>
- Koutsarnakis C et al (2019) Sledge runner fasciculus: anatomic architecture and tractographic morphology. *Brain Struct Funct*. <https://doi.org/10.1007/s00429-018-01822-4>
- Krumbholz K, Schönwiesner M, von Cramon DY, Rübsem R, Shah NJ, Zilles K, Fink GR (2004) Representation of interaural temporal information from left and right auditory space in the human planum temporale and inferior parietal lobe. *Cereb Cortex* 15:317–324
- Lambon Ralph MA, Patterson K (2008) Generalization and differentiation in semantic memory: insights from semantic dementia. *Ann NY Acad Sci* 1124:61–76
- Lambon Ralph MA, Lowe C, Rogers TT (2007) Neural basis of category-specific semantic deficits for living things: evidence from semantic dementia, HSVE and a neural network model. *Brain* 130:1127–1137
- Lambon Ralph MA, Pobric G, Jefferies E (2008) Conceptual knowledge is underpinned by the temporal pole bilaterally: convergent evidence from rTMS. *Cereb Cortex* 19:832–838

- Le Bihan D, Mangin JF, Poupon C, Clark CA, Pappata S, Molko N, Chabriat H (2001) Diffusion tensor imaging: concepts and applications. *J Magn Reson Imaging* 13:534–546
- Le Bihan D, Poupon C, Amadon A, Lethimonnier F (2006) Artifacts and pitfalls in diffusion MRI. *J Magn Reson Imaging* 24:478–488. <https://doi.org/10.1002/jmri.20683>
- Lewald J, Getzmann S (2011) When and where of auditory spatial processing in cortex: a novel approach using electrotopography. *PLoS One* 6:e25146. <https://doi.org/10.1371/journal.pone.0025146>
- Liakos F, Koutsarnakis C (2016) The role of white matter dissection technique in modern neuroimaging: can neuroradiologists benefit from its use? *Surg Radiol Anat* 38:275
- Liegeois-Chauvel C, Musolino A, Chauvel P (1991) Localization of the primary auditory area in man. *Brain* 114(Pt 1A):139–151
- Logothetis NK, Pauls J, Augath M, Trinath T, Oeltermann A (2001) Neurophysiological investigation of the basis of the fMRI signal. *Nature* 412:150
- Lomber SG, Malhotra S (2008) Double dissociation of ‘what’ and ‘where’ processing in auditory cortex. *Nat Neurosci* 11:609
- Macaluso E, Driver J, Frith CD (2003) Multimodal spatial representations engaged in human parietal cortex during both saccadic and manual spatial orienting. *Curr Biol* 13:990–999
- Makris N, Pandya DN (2009) The extreme capsule in humans and rethinking of the language circuitry. *Brain Struct Funct* 213:343–358. <https://doi.org/10.1007/s00429-008-0199-8>
- Makris N, Meyer JW, Bates JF, Yeterian EH, Kennedy DN, Caviness VS (1999) MRI-Based topographic parcellation of human cerebral white matter and nuclei II. Rationale and applications with systematics of cerebral connectivity. *Neuroimage* 9:18–45. <https://doi.org/10.1006/nimg.1998.0384>
- Makris N, Kennedy DN, McInerney S, Sorensen AG, Wang R, Caviness VS Jr, Pandya DN (2004) Segmentation of subcomponents within the superior longitudinal fascicle in humans: a quantitative, in vivo, DT-MRI study. *Cereb Cortex* 15:854–869
- Makris N, Kennedy DN, McInerney S, Sorensen AG, Wang R, Caviness VS Jr, Pandya DN (2005) Segmentation of subcomponents within the superior longitudinal fascicle in humans: a quantitative, in vivo, DT-MRI study. *Cereb Cortex* 15:854–869. <https://doi.org/10.1093/cercor/bhh186>
- Makris N, Papadimitriou GM, Kaiser JR, Sorg S, Kennedy DN, Pandya DN (2009) Delineation of the middle longitudinal fascicle in humans: a quantitative, in vivo, DT-MRI study. *Cereb Cortex* 19:777–785. <https://doi.org/10.1093/cercor/bhn124>
- Makris N et al (2013a) Human middle longitudinal fascicle: variations in patterns of anatomical connections. *Brain Struct Funct* 218:951–968. <https://doi.org/10.1007/s00429-012-0441-2>
- Makris N et al (2013b) Human middle longitudinal fascicle: segregation and behavioral-clinical implications of two distinct fiber connections linking temporal pole and superior temporal gyrus with the angular gyrus or superior parietal lobule using multi-tensor tractography. *Brain Imaging Behav* 7:335–352. <https://doi.org/10.1007/s11682-013-9235-2>
- Makris N et al (2017) Mapping temporo-parietal and temporo-occipital cortico-cortical connections of the human middle longitudinal fascicle in subject-specific, probabilistic, and stereotaxic Talairach spaces. *Brain Imaging Behav* 11:1258–1277. <https://doi.org/10.1007/s11682-016-9589-3>
- Maldjian JA, Laurienti PJ, Kraft RA, Burdette JH (2003) An automated method for neuroanatomic and cytoarchitectonic atlas-based interrogation of fMRI data sets. *Neuroimage* 19:1233–1239
- Maldonado IL, de Champfleury NM, Velut S, Destrieux C, Zemmoura I, Duffau H (2013) Evidence of a middle longitudinal fasciculus in the human brain from fiber dissection. *J Anat* 223(1):38–45. <https://doi.org/10.1111/joa.12055>
- Mandonnet E, Sarubbo S, Petit L (2018) The nomenclature of human white matter association pathways: proposal for a systematic taxonomic anatomical classification. *Front Neuroanat* 12:94. <https://doi.org/10.3389/fnana.2018.00094>
- Martino J et al (2011) Cortex-sparing fiber dissection: an improved method for the study of white matter anatomy in the human brain. *J Anat* 219:531–541
- Martino J, De Witt Hamer PC, Berger MS, Lawton MT, Arnold CM, de Lucas EM, Duffau H (2013) Analysis of the subcomponents and cortical terminations of the perisylvian superior longitudinal fasciculus: a fiber dissection and DTI tractography study. *Brain Struct Funct* 218:105–121. <https://doi.org/10.1007/s00429-012-0386-5>
- Matsumoto R et al (2008) Hemispheric asymmetry of the arcuate fasciculus: a preliminary diffusion tensor tractography study in patients with unilateral language dominance defined by Wada test. *J Neurol* 255:1703–1711. <https://doi.org/10.1007/s00415-008-0005-9>
- Mazziotta J et al (2001) A probabilistic atlas and reference system for the human brain: International Consortium for Brain Mapping (ICBM). *Philos Trans R Soc Lond Ser B Biol Sci* 356:1293–1322
- Menjot de Champfleury N, Lima Maldonado I, Moritz-Gasser S, Machi P, Le Bars E, Bonafe A, Duffau H (2013) Middle longitudinal fasciculus delineation within language pathways: a diffusion tensor imaging study in human. *Eur J Radiol* 82:151–157. <https://doi.org/10.1016/j.ejrad.2012.05.034>
- Monroy-Sosa A et al (2019) Microsurgical anatomy of the vertical rami of the superior longitudinal fasciculus: an intraparietal sulcus dissection study. *Oper Neurosurg (Hagerstown)* 16:226–238. <https://doi.org/10.1093/ons/opy077>
- Mori S, Zhang J (2006) Principles of diffusion tensor imaging and its applications to basic neuroscience research. *Neuron* 51:527–539. <https://doi.org/10.1016/j.neuron.2006.08.012>
- Mummery CJ, Patterson K, Price CJ, Ashburner J, Frackowiak RS, Hodges JR (2000) A voxel-based morphometry study of semantic dementia: relationship between temporal lobe atrophy and semantic memory. *Ann Neurol* 47:36–45
- Nachtergaele P et al (2019) The temporoinsular projection system: an anatomical study. *J Neurosurg*. <https://doi.org/10.3171/2018.11.jns18679>
- Nestor PJ, Fryer TD, Hodges JR (2006) Declarative memory impairments in Alzheimer’s disease and semantic dementia. *Neuroimage* 30:1010–1020
- Nimsky C, Bauer M, Carl B (2016) Merits and limits of tractography techniques for the uninitiated. *Adv Tech Stand Neurosurg*. https://doi.org/10.1007/978-3-319-21359-0_2
- Noppeney U et al (2007) Temporal lobe lesions and semantic impairment: a comparison of herpes simplex virus encephalitis and semantic dementia. *Brain* 130:1138–1147
- Obleser J et al (2006) Vowel sound extraction in anterior superior temporal cortex. *Hum Brain Mapp* 27:562–571
- Oouchi H, Yamada K, Sakai K, Kizu O, Kubota T, Ito H, Nishimura T (2007) Diffusion anisotropy measurement of brain white matter is affected by voxel size: underestimation occurs in areas with crossing fibers. *AJNR Am J Neuroradiol* 28:1102–1106. <https://doi.org/10.3174/ajnr.A0488>
- Palm C et al (2010) Towards ultra-high resolution fibre tract mapping of the human brain—registration of polarised light images and reorientation of fibre vectors. *Front Hum Neurosci* 4:9
- Panesar SS, Yeh FC, Jacquesson T, Hula W, Fernandez-Miranda JC (2018) A quantitative tractography study into the connectivity, segmentation and laterality of the human inferior longitudinal fasciculus. *Front Neuroanat* 12:47. <https://doi.org/10.3389/fnana.2018.00047>
- Pescatori L, Tropeano MP, Manfreda A, Delfini R, Santoro A (2017) Three-dimensional anatomy of the white matter fibers of the

- temporal lobe: surgical implications. *World Neurosurg* 100:144–158. <https://doi.org/10.1016/j.wneu.2016.12.120>
- Petrides M (2012) The human cerebral cortex an MRI atlas of the Sulci and Gyri in MNI stereotaxic space. Academic Press, Oxford
- Petrides M, Pandya DN (1984) Projections to the frontal cortex from the posterior parietal region in the rhesus monkey. *J Comp Neurol* 228:105–116. <https://doi.org/10.1002/cne.902280110>
- Pierpaoli C, Basser PJ (1996) Toward a quantitative assessment of diffusion anisotropy Magnetic resonance in medicine 36:893–906
- Pobric G, Jefferies E, Ralph MAL (2007) Anterior temporal lobes mediate semantic representation: mimicking semantic dementia by using rTMS in normal participants. *Proc Natl Acad Sci* 104:20137–20141
- Poremba A, Saunders RC, Crane AM, Cook M, Sokoloff L, Mishkin M (2003) Functional mapping of the primate auditory system. *Science* 299:568–572. <https://doi.org/10.1126/science.1078900>
- Poremba A, Malloy M, Saunders RC, Carson RE, Herscovitch P, Mishkin M (2004) Species-specific calls evoke asymmetric activity in the monkey's temporal poles. *Nature* 427:448–451. <https://doi.org/10.1038/nature02268>
- Price CJ (2000) The anatomy of language: contributions from functional neuroimaging. *J Anat* 197:335–359
- Raichle ME (2009) A brief history of human brain mapping. *Trends Neurosci* 32:118–126
- Rauschecker JP, Scott SK (2009) Maps and streams in the auditory cortex: nonhuman primates illuminate human speech processing. *Nat Neurosci* 12:718–724. <https://doi.org/10.1038/nn.2331>
- Rauschecker JP, Tian B (2000) Mechanisms and streams for processing of “what” and “where” in auditory cortex. *Proc Natl Acad Sci USA* 97:11800–11806. <https://doi.org/10.1073/pnas.97.22.11800>
- Rhoton AL Jr (2002) The cerebrum. *Neurosurgery* 51:S1-1–S1-52
- Rilling JK, Glasser MF, Preuss TM, Ma X, Zhao T, Hu X, Behrens TE (2008) The evolution of the arcuate fasciculus revealed with comparative DTI. *Nat Neurosci* 11:426–428. <https://doi.org/10.1038/nn2072>
- Romanski LM, Bates JF, Goldman-Rakic PS (1999) Auditory belt and parabelt projections to the prefrontal cortex in the rhesus monkey. *J Comp Neurol* 403:141–157
- Roux F-E, Minkin K, Durand J-B, Sacko O, Réhault E, Tanova R, Démonet J-F (2015) Electrostimulation mapping of comprehension of auditory and visual words. *Cortex* 71:398–408
- Sarubbo S, De Benedictis A, Merler S, Mandonnet E, Balbi S, Granieri E, Duffau H (2015) Towards a functional atlas of human white matter. *Hum Brain Mapp* 36:3117–3136. <https://doi.org/10.1002/hbm.22832>
- Schmahmann JD, Pandya DN (2007) Cerebral white matter—historical evolution of facts and notions concerning the organization of the fiber pathways of the brain. *J Hist Neurosci* 16:237–267. <https://doi.org/10.1080/09647040500495896>
- Schmahmann JD, Pandya DN, Wang R, Dai G, D'arceuil HE, de Crespigny AJ, Wedeen VJ (2007) Association fibre pathways of the brain: parallel observations from diffusion spectrum imaging and autoradiography. *Brain* 130:630–653
- Seehaus A et al (2015) Histological validation of high-resolution DTI in human post mortem tissue. *Front Neuroanat* 9:98. <https://doi.org/10.3389/fnana.2015.00098>
- Seltzer B, Pandya DN (1978) Afferent cortical connections and architectonics of the superior temporal sulcus and surrounding cortex in the rhesus monkey. *Brain Res* 149:1–24
- Seltzer B, Pandya DN (1984) Further observations on parieto-temporal connections in the rhesus monkey. *Exp Brain Res* 55:301–312
- Seltzer B, Pandya DN (1991) Post-rolandic cortical projections of the superior temporal sulcus in the rhesus monkey. *J Comp Neurol* 312:625–640. <https://doi.org/10.1002/cne.903120412>
- Setsonpop K et al (2013) Pushing the limits of in vivo diffusion MRI for the Human Connectome Project. *Neuroimage* 80:220–233. <https://doi.org/10.1016/j.neuroimage.2013.05.078>
- Shah A, Goel A, Jhawar SS, Patil A, Rangnekar R, Goel A (2019) Neural circuitry: architecture and function—a fiber dissection study. *World Neurosurg* 125:e620–e638. <https://doi.org/10.1016/j.wneu.2019.01.139>
- Shrout PE, Fleiss JL (1979) Intraclass correlations: uses in assessing rater reliability. *Psychol Bull* 86:420–428
- Sporns O, Tononi G, Kötter R (2005) The human connectome: a structural description of the human brain. *PLoS Comput Biol* 1:e42
- Takao H, Hayashi N, Kabasawa H, Ohtomo K (2012) Effect of scanner in longitudinal diffusion tensor imaging studies. *Hum Brain Mapp* 33:466–477. <https://doi.org/10.1002/hbm.21225>
- Tata MS, Ward LM (2005a) Early phase of spatial mismatch negativity is localized to a posterior “where” auditory pathway. *Exp Brain Res* 167:481–486
- Tata MS, Ward LM (2005b) Spatial attention modulates activity in a posterior “where” auditory pathway. *Neuropsychologia* 43:509–516
- Thomas C, Ye FQ, Irfanoglu MO, Modi P, Saleem KS, Leopold DA, Pierpaoli C (2014) Anatomical accuracy of brain connections derived from diffusion MRI tractography is inherently limited. *Proc Natl Acad Sci USA* 111:16574–16579. <https://doi.org/10.1073/pnas.1405672111>
- Tian B, Reser D, Durham A, Kustov A, Rauschecker JP (2001) Functional specialization in rhesus monkey auditory cortex. *Science* 292:290–293
- Tremblay P, Perron M, Deschamps I, Kennedy-Higgins D, Houde JC, Dick AS, Descoteaux M (2019) The role of the arcuate and middle longitudinal fasciculi in speech perception in noise in adulthood. *Hum Brain Mapp* 40:226–241. <https://doi.org/10.1002/hbm.24367>
- Ture U, Yasargil MG, Friedman AH, Al-Mefty O (2000) Fiber dissection technique: lateral aspect of the brain. *Neurosurgery* 47(2):417–426 (**discussion 417–426**)
- Veenith TV et al (2013) Inter subject variability and reproducibility of diffusion tensor imaging within and between different imaging sessions. *PLoS One* 8:e65941. <https://doi.org/10.1371/journal.pone.0065941>
- Visser M, Jefferies E, Lambon Ralph M (2010) Semantic processing in the anterior temporal lobes: a meta-analysis of the functional neuroimaging literature. *J Cognit Neurosci* 22:1083–1094
- Vos SB, Jones DK, Viergever MA, Leemans A (2011) Partial volume effect as a hidden covariate in DTI analyses. *Neuroimage* 55:1566–1576. <https://doi.org/10.1016/j.neuroimage.2011.01.048>
- Wakana S et al (2007) Reproducibility of quantitative tractography methods applied to cerebral white matter. *Neuroimage* 36:630–644. <https://doi.org/10.1016/j.neuroimage.2007.02.049>
- Wang H et al (2011) Reconstructing micrometer-scale fiber pathways in the brain: multi-contrast optical coherence tomography based tractography. *Neuroimage* 58:984–992
- Wang Y, Fernandez-Miranda JC, Verstynen T, Pathak S, Schneider W, Yeh FC (2013) Rethinking the role of the middle longitudinal fascicle in language and auditory pathways. *Cereb Cortex* 23:2347–2356. <https://doi.org/10.1093/cercor/bhs225>
- Warren JD, Griffiths TD (2003) Distinct mechanisms for processing spatial sequences and pitch sequences in the human auditory brain. *J Neurosci* 23:5799–5804
- Warren JD, Zielinski BA, Green GG, Rauschecker JP, Griffiths TD (2002) Perception of sound-source motion by the human brain. *Neuron* 34:139–148
- Wu Y, Sun D, Wang Y, Wang Y, Wang Y (2016) Tracing short connections of the temporo-parieto-occipital region in the human brain

- using diffusion spectrum imaging and fiber dissection. *Brain Res* 1646:152–159. <https://doi.org/10.1016/j.brainres.2016.05.046>
- Yang Z, Qiu J, Wang P, Liu R, Zuo XN (2016) Brain structure-function associations identified in large-scale neuroimaging data. *Brain Struct Funct* 221:4459–4474. <https://doi.org/10.1007/s00429-015-1177-6>
- Zimmer U, Macaluso E (2005) High binaural coherence determines successful sound localization and increased activity in posterior auditory areas. *Neuron* 47:893–905

Publisher's Note Springer Nature remains neutral with regard to jurisdictional claims in published maps and institutional affiliations.